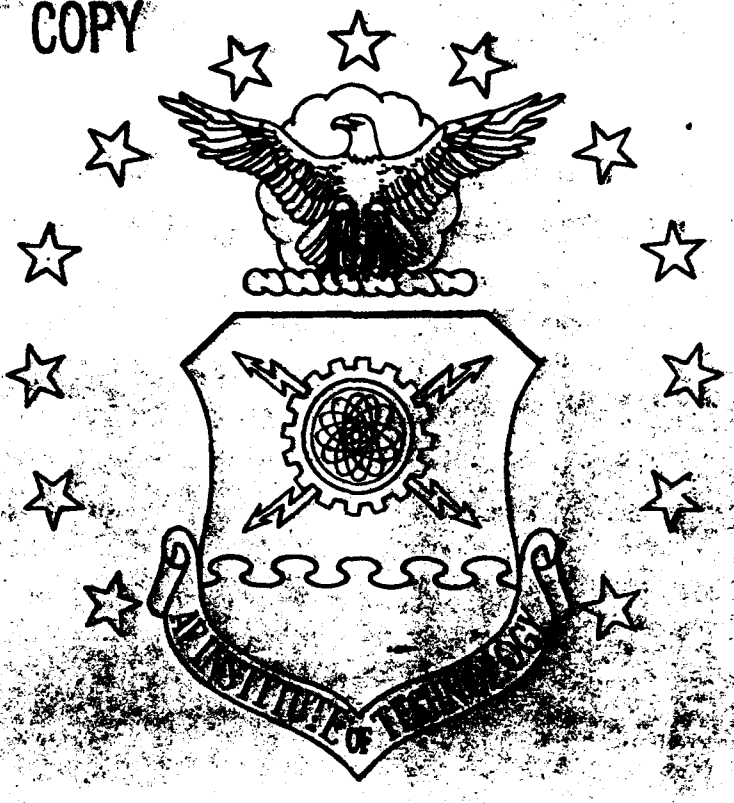

FINITE ELEMENT INVESTIGATION INTO THE DYNAMIC INSTABILITY CHARACTERISTICS OF LAMINATED COMPOSITE PANELS

THESIS

Walter W. Taylor Jr
Major, USAF

DEPARTMENT OF THE AIR FORCE
AIR UNIVERSITY
AIR FORCE INSTITUTE OF TECHNOLOGY

AFIT/GAE/ENY/90D-28

FINITE ELEMENT INVESTIGATION INTO THE DYNAMIC INSTABILITY CHARACTERISTICS OF LAMINATED COMPOSITE PANELS

THESIS

Walter W. Taylor Jr
Major, USAF

AFIT/GAE/ENY/90D-28

AFIT/GAE/ENY/90D-28

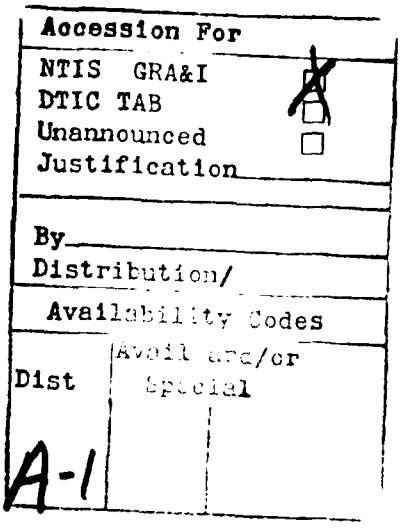

FINITE ELEMENT INVESTIGATION INTO THE DYNAMIC INSTABILITY CHARACTERISTICS OF LAMINATED COMPOSITE PANELS

THESIS

Presented to the Faculty of the School of Engineering

of the Air Force Institute of Technology

Air University

In Partial Fulfillment of the

Requirements for the Degree of

Master of Science in Aeronautical Engineering

Walter W. Taylor Jr

Major, USAF

December, 1990

Acknowledgements

This thesis is part of a research project on the static and dynamic response of composite shells sponsored by the Air Force Office of Scientific Research, Dr. Spencer Wu contract monitor; Dr. Anthony Palazotto, AFIT/ENY, principal investigator.

I wish to thank Dr. Palazotto for his expertise and guidance throughout this research; Major Scott Dennis (Ph.D.) who authored the computer code used in my investigation; Dr. C.T. Tsai who programmed the solution algorithm and incorporated the dynamic solver into the code; and the many other AFIT faculty and staff who made my educational experience a memorable one.

Special thanks go to my wife Denise for keeping me in touch with reality and without whose help I would never have found the "on" switch on our computer.

As a final note I would like to remember Captain Wayne Wilsdon, a fellow classmate, officer and friend whose untimely death during our stay at AFIT makes one realize that there are more important things in life than homework, tests, and grades.

Contents

List of Figures

List of Symbols

A, D, F	linear and two higher order stiffness matrices
a, b	isoparametric element half dimensions in ξ, η directions
C_{ij}	unreduced constitutive matrix term
E	Young's (elastic) modulus
ϵ, ϵ^o	strain, strain of middle surface
$\mathscr{E}$, $\mathscr{E}^o$	vector of ϵ, ϵ^o strain terms
F	external force vector
G	shear modulus
χ	Hermitian shape function
h	shell thickness
h_i	general coordinate system scale factors
K, N_1, N_2	constant, first, and higher order stiffness matrices
K_T	tangent stiffness matrix
N, Q	linear, quadratic Lagrangian shape functions
P	applied load vector
Q_{ij}	lamina reduced stiffness matrix element
$\bar{Q}_{ij}$	transformed reduced lamina stiffness
q	nodal displacement vector
R	radius of curvature
Δs	increment along equilibrium path for Riks solver
T	transformation matrix

m	order of the beta-m method
M	consistent mass matrix
C	damping matrix
E	strain energy
W, W_e	external work
x, s, z	shell coordinates (longitudinal, circumferential, transverse)
u	longitudinal (x-axis) displacement
v	circumferential (s-axis) displacement
w	transverse (z-axis) displacement
u^o, v_o, w	displacement of datum surface
θ	opening angle of cylindrical panel arc
ϕ	angle of ply fibers to shell x-axis
ψ	shear deformation of shell normal about i-axis at middle surface
χ_{ij}	out of plane strain terms
X	matrix of out of plane strain terms χ_{ij}
Π_p	potential energy
ν	Poisson's ratio
σ	stress
Ω	shell middle surface designator
λ_i	load fraction for solution step i in Riks solver
δ	variation operator
t	time
ρ	mass density

$U^{(0)}$	displacement
$U^{(1)}$	velocity
$U^{(2)}$	acceleration

Abstract

The dynamic instability characteristics of a laminated composite panel subjected to a transverse load is studied in this research. Up to cubic variations in the thickness coordinate are included in the inplane displacement field, and only the constant component is kept in the transverse displacement. The transverse shear strains retain only linear displacement terms and vary parabolically through the thickness vanishing at the top and bottom surfaces. The complete quadratic displacement functions are included in the inplane strains to characterize the large displacements/rotations response during a snapping process. A 36 degree of freedom shell element is used to obtain numerical results.

The static snap through load versus displacement curve, as well as the critical collapse load, is first examined by invoking the Riks technique along with the Newton-Raphson iteration scheme at each load increment level. The beta-m time marching integration method is then employed to evaluate a dynamic response. Two step loads, with the step magnitude slightly below and above the critical collapse load, are introduced in the dynamic analysis. Moreover, the damping effect is incorporated to

yield a steady-state solution. The response resulting from the dynamic steady-state analysis subjected to a step load matches the displacement on the snap through load versus displacement curve.

FINITE ELEMENT INVESTIGATION INTO THE DYNAMIC INSTABILITY CHARACTERISTICS OF LAMINATED COMPOSITE PANELS

I. INTRODUCTION

Laminated composite materials are seeing widespread use in many diverse industries. One of these is the aerospace industry where, due to the need to minimize weight, complex shell configurations are common structural elements. Structural components made from composite materials typically have higher strength and stiffness to weight ratios than those made from isotropic materials. In addition, composite materials' properties can be tailored to meet specific design goals. Increased stiffness and strength are designed only where needed. However, optimized structural systems are often more susceptible to instabilities such as buckling, collapse, or vibration, especially if the composite is a thin shell and the load is applied in the transverse direction. The purpose of this

research is to investigate numerically the static and dynamic response of a laminated graphite/epoxy composite cylindrical shell (curved panel) subjected to transverse loading.

Analytical Method

The computer program SHELL was used exclusively in this research. It was originally developed by Dennis (9) for large displacement/rotation static analysis of shell structures. The modified Riks-Wempner solution algorithm was added to the program by Tsai and Palazotto (26) and it was extended for the study of non-linear vibrations of cylindrical shells also by Tsai and Palazotto (14). The uniqueness of the SHELL program is that parabolic shear strains are assumed to vary through the shell thickness and vanish at the top and bottom surface. Although classical plate and shell theory for thin isotropic structures ignore shear stress through the thickness, it is not appropriate to do so with composite shells. The coupling of extensional, bending, and shear strain must be taken into consideration.

It also should be noted that the SHELL program incorporates material linearity. This is appropriate because in structural applications, materials are normally restricted to the linear elastic region. This implies that any fiber or ply breakage during large rotations and

displacements is ignored.

SHELL offers two strain displacement formulation options for a cylindrical shell finite element. When Dennis originally wrote the code, he incorporated the Donnell shell equations along with the non-linear equations he developed in order for comparisons to be made. Only Dennis' non-linear option is used in this research.

The analytical approach taken in this work is to use both the static and dynamic analytical capabilities of SHELL to do collapse analysis of circular shells and arches subjected to transverse loading. Comparisons to other work is done when applicable. In the interest of semantics, it should be noted that the terms buckling, collapse, and snap-through are all used interchangeably.

Previous Work

The engineering analysis of general shells goes back no further than the start of the twentieth century. Simmons (24) notes that in 1920, A. E. Love published a set of equations for the midsurface displacement of circular, cylindrical thin shells. Perhaps the first useful cylindrical shell equations were presented by Donnell (10) in 1933. He determined (both analytically and experimentally) that circumferentially trigonometric deformations with small wavelengths allow one to discard

several terms in the curvature and twist equations. The complexity of the resulting expressions are on the order of the Von Karman plate equations. The primary restriction is that the ratio of shell thickness must be small and if rotations of the midsurface greater than fifteen degrees occur then accuracy suffers.

Another major milestone in shell theory occurred in 1959 by Sanders (22). He assumed that transverse shear strains are negligible and solved for the corresponding transverse shear stress resultants, thus partially incorporating transverse effects. The significant improvement over Love's approximations is that by considering rotation of the shell normal, but neglecting rotations about this normal, Sanders' relations allow for small strain free rigid body motion.

Since finite element analysis came into being for use in structural analysis, many researchers have developed finite elements for cylindrical shells. Most applicable to the present research is the work done by Saber and Lock (21), which employed a solution algorithm capable of tracing the post-collapse behavior by incrementing either load or displacement to avoid numerical singularity at critical points. A 20 degree of freedom curved rectangular element for an isotropic material was used. Most theoretical work done up until this point in time involved isotropic

materials. With the advent of composites, it was necessary to extend first-order theory to laminated materials. Chung and Widera (4) expanded Donnell's equations for use with laminated composites. It should be noted that the limits of the applicability of the theory as far as magnitude of deformations are concerned remained the same.

All work reported up to this point is considered first-order theory. The development of a higher order theory incorporating transverse effects was driven by the need to accurately analyze laminated composite shells which typically have more severe transverse stresses. Dennis (8) and Reddy and Liu (17) have both presented comparable higher order theories incorporating transverse effects, of which Dennis' is the basis for the present work. This theory allows for fully non-linear in-plane strains, but only linear transverse shear strain-displacement relations. The acceptability of a linear transverse strain field in a non-linear theory is justified by noting that transverse effects are small compared to in-plane effects, thus smaller higher-order terms of the already small transverse terms are negligible (9).

The solution method for geometrically non-linear problems by the finite element method requires recalculation of the structure's stiffness matrix as it changes during deformation. The Newton-Raphson method for iteration is

widely used in such computations. However, once the structure has reached its peak load, it has essentially zero stiffness and inverting the stiffness matrix as required for load-controlled Newton-Raphson iteration to converge to the equilibrium solution is impossible. This problem has been circumvented by reformulating the equilibrium equations to step by displacement rather than load when a peak load was encountered, and using the usual load incrementing method to step through areas of zero or reversing incremental displacement. A solution algorithm without the need to swap between methods was developed by Riks (18,19) and Wemper (27) and applied to structural problems by Crisfield (7). In it, a selected arc length of the equilibrium path is incremented rather than load or displacement. Since step size does not decrease to zero due to convergence to a peak load or peak displacement point as the former methods do, this technique steps past such singular areas and allows uninterrupted tracing of the equilibrium path (15). Tsai and Palazotto (14) have applied this solution algorithm to the SHELL computer code used in this research.

Although a great deal of research has been done into the static analysis of shell structures, the development of the finite element method for nonlinear shell dynamic analysis has not been as rapid. Clough and Wilson (5) have done work into nonlinear vibrations using flat plate

elements. The higher order transverse shear deformation theory used in this research has been extended for the study of nonlinear vibration of cylindrical shells by Tsai and Palazotto (26).

Current Work

The subject of this research is the dynamic response to a transverse point load of a laminated cylindrical shell and arch. The static and dynamic analysis capabilities of the SHELL computer code are further explored. Both dynamic and static analysis of the post buckling response of cylindrical shells are compared. No experiment or comparable numerical study could be found with which to compare results; hence trends and general conclusions will be compared with conclusions in some of the studies referenced above. The computers used were an Elxsi 6400 using the Unix operating system located at the Air Force Institute of Technology and a Cray Y-MP8/864 running Unicos located at the Ohio Supercomputer Center, the Ohio State University.

II. THEORY

In order for the reader to better understand the theoretical basis for the data presented later, the finite element formulations governing the SHELL computer code is now discussed. The geometry and assumptions used in the model will be presented along with the constitutive development, the strain-displacement relations and the potential energy theory used to develop the equations of motion. The resulting 36 DOF element will be presented. Finally, the extension of the code to dynamic analysis by Tsai and Palazotto (14) will be discussed.

Bathe and Ho (2) stated the following set of criteria for a desirable shell element:

1.) No spurious zero-energy modes should exist, so that reliable results can always be expected. No numerical fudge factors should be necessary, either.

2.) The element should be applicable to general shell structures, including those with beam stiffeners, cutouts, intersections, etc.

3.) The element should be cost-effective for linear as well as nonlinear static and dynamic analysis. This implies that the degrees of freedom is held to a minimum. It should allow analysis of large

displacement and large rotation problems, and materially nonlinear situations.

Criterion 1 is achieved in this formulation. The code has not been developed beyond the research stage, so application to other than plate and cylindrical shell cases modeled with rectangular elements is not yet possible. However, the underlying theory by which transverse shear is incorporated is not restricted geometrically, so criterion 2 is somewhat met. Material linearity is assumed in the formulation of the element, so criterion 3 is only partially fulfilled. The incorporation of through the thickness shear effects in a shell structure, while maintaining a two dimensional analysis, satisfies the first part of this criterion.

Geometry and Assumptions

The curvilinear orthogonal coordinate system and nomenclature used in this formulation of the laminated cylindrical shell is shown in Fig (2-1). The x-axis lies along the straight dimension of the panel; the s-axis follows the circumference, and the z-axis is everywhere normal to the shell middle surface, positive toward the center of curvature. The surface formed by the x and s axes lies in the center of the thickness of the panel, so the thickness coordinate is negative on the outer surface and positive on the inner surface. Displacements along the x,s

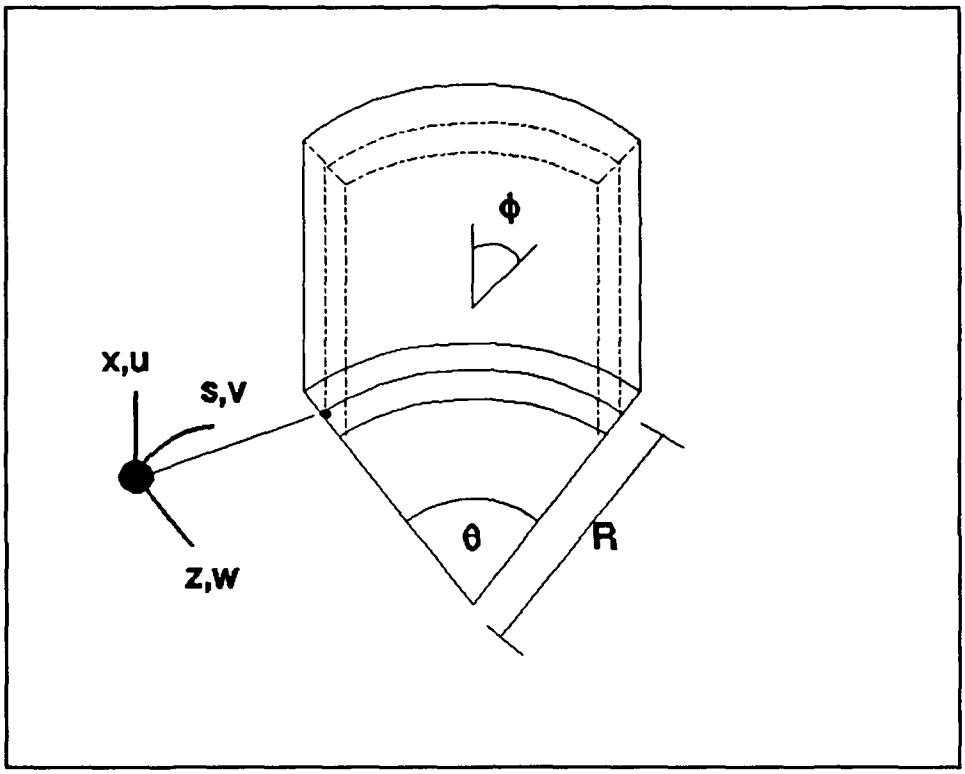

Figure 2-1. Cylindrical Shell Geometry

and z axes are u, v and w respectively. In the early vectorial development, the coordinate θ is used instead of s for the purpose of generality and s is used when specializing to the cylindrical geometry. Since the structure analyzed here is an open shell, the angle θ is also useful for describing shallowness. The angle ϕ specifies the orientation angle of each ply in the laminate. Subscripts denoting stress and strain orientation are explained in Table 2-1 and Fig (2-2).

Table 2-1. SHELL Contracted Notation

STRESS		STRAIN		CYLINDRICAL COORDINATES
EXPLICIT	CONTRACTED	EXPLICIT	CONTRACTED	
σ_{11}	σ_1	ϵ_{11}	ϵ_1	x → 1
σ_{22}	σ_2	ϵ_{22}	ϵ_2	s → 2
σ_{33}	σ_3	ϵ_{33}	ϵ_3	z → 3
σ_{23}	σ_4	$2\epsilon_{23}=\gamma_{23}$	ϵ_4	s-z → 4
σ_{13}	σ_5	$2\epsilon_{13}=\gamma_{13}$	ϵ_5	x-z → 5
σ_{12}	σ_6	$2\epsilon_{12}=\gamma_{12}$	ϵ_6	x-s → 6

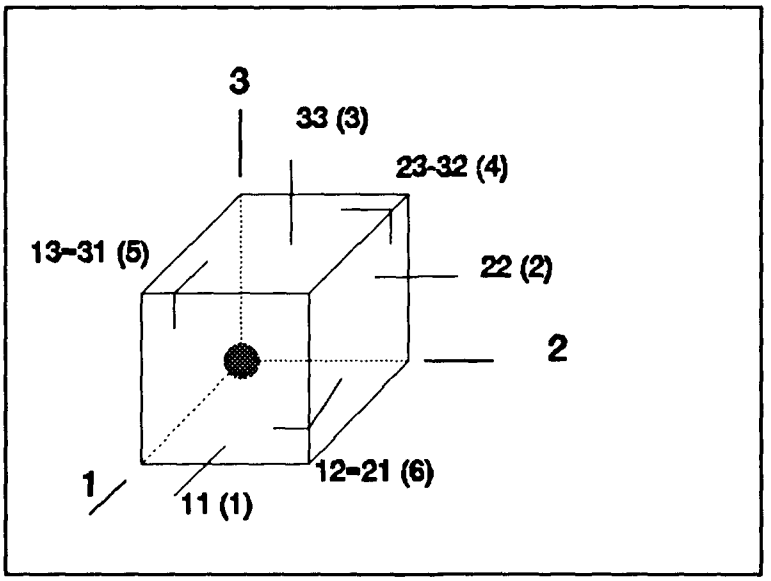

Figure 2-2. Fiber Reinforced Lamina Definitions

Constitutive Development

In this section the stress-strain relations for a laminate of arbitrarily oriented transversely isotropic plies will be developed. The main difference from isotropic relations is the summation over the lamina thickness of the directional constitutive equations for each ply, arriving at the total laminate's effective stress-strain relation. This section follows the references by Silva (23) and Dennis (8).

For an isotropic material, stress σ and strain ϵ are related as

$$\sigma = E\,\epsilon \tag{2-1}$$

where E is Young's modulus. When considering the general case of an anisotropic material, Young's modulus can differ with different load orientations so this equation expands to

$$\begin{Bmatrix} \sigma_1 \\ \sigma_2 \\ \sigma_3 \\ \sigma_4 \\ \sigma_5 \\ \sigma_6 \end{Bmatrix} = \begin{Bmatrix} C_{11} & C_{12} & C_{13} & C_{14} & C_{15} & C_{16} \\ C_{21} & C_{22} & C_{23} & C_{24} & C_{25} & C_{26} \\ C_{31} & C_{32} & C_{33} & C_{34} & C_{35} & C_{36} \\ C_{41} & C_{42} & C_{43} & C_{44} & C_{45} & C_{46} \\ C_{51} & C_{52} & C_{53} & C_{54} & C_{55} & C_{56} \\ C_{61} & C_{62} & C_{63} & C_{64} & C_{65} & C_{66} \end{Bmatrix} \begin{Bmatrix} \epsilon_1 \\ \epsilon_2 \\ \epsilon_3 \\ \epsilon_4 \\ \epsilon_5 \\ \epsilon_6 \end{Bmatrix} \tag{2-2}$$

where C_{ij} is the stiffness matrix of 36 terms defining the stress-strain relationship for loading in the i^{th} direction. If one only considers the energy conserving elastic region,

the matrix C_{ij} is symmetric; i.e. $C_{12} = C_{21}$ and so forth, resulting in 21 independent terms. In the case of a directional fiber-reinforced composite material (the material in this research), the three mutually orthogonal planes of symmetry decouple shear strains from normal stresses and vice versa. This defines an orthotropic material, which has only 9 independent stiffnesses.

$$\begin{Bmatrix} \sigma_1 \\ \sigma_2 \\ \sigma_3 \\ \sigma_4 \\ \sigma_5 \\ \sigma_6 \end{Bmatrix} = \begin{bmatrix} C_{11} & C_{12} & C_{13} & 0 & 0 & 0 \\ C_{12} & C_{22} & C_{23} & 0 & 0 & 0 \\ C_{13} & C_{23} & C_{33} & 0 & 0 & 0 \\ 0 & 0 & 0 & C_{44} & 0 & 0 \\ 0 & 0 & 0 & 0 & C_{55} & 0 \\ 0 & 0 & 0 & 0 & 0 & C_{66} \end{bmatrix} \begin{Bmatrix} \epsilon_1 \\ \epsilon_2 \\ \epsilon_3 \\ \epsilon_4 \\ \epsilon_5 \\ \epsilon_6 \end{Bmatrix} \qquad (2\text{-}3)$$

Also, since such a material responds equally to any direction of load in the plane perpendicular to the fiber longitudinal axis (2-3 plane), the 2 and 3 subscripts are interchangeable. This behavior is called transverse isotropy and further reduces the number of independent stiffness terms to seven. Thus, in terms of engineering constants E (Young's modulus) and ν (Poisson's ratio) the following are the stiffness terms:

$$C_{11}=E_1\frac{1-\nu_{23}^2}{\Delta}$$

$$C_{22}=C_{33}=E_2\frac{1-\nu_{12}\nu_{21}}{\Delta}$$

$$C_{12}=C_{13}=E_1\nu_{21}\frac{1+\nu_{23}}{\Delta} \qquad (2\text{-}4)$$

$$C_{23}=E_2\frac{\nu_{23}+\nu_{12}\nu_{21}}{\Delta}$$

$$C_{44}=G_{23}$$

$$C_{55}=G_{31}$$

$$C_{66}=G_{12}$$

where $\Delta = 1-2\nu_{12}\nu_{21}-\nu_{23}^2-2\nu_{12}\nu_{21}\nu_{23}$, E_1 is Young's modulus for loads along the 1 axis, G_{12} is the shear modulus in the 1-2 plane, and ν_{12} denotes the ratio of strains ϵ_2/ϵ_1 for stress applied in the 1 direction.

Due to the fact that in most composite materials the plies are thin, the assumptions of plane stress ($\sigma_3=\sigma_4=\sigma_5=0$) is usually made at this point. However, in the SHELL code, non-zero through the thickness shear stress is allowed, thus a "modified" state of plane stress is assumed in which only $\sigma_3=0$. Solving for ϵ_3 in Eq (2-3) after applying this assumption yields

$$\epsilon_3 = -\frac{C_{13}}{C_{33}}\epsilon_1 - \frac{C_{23}}{C_{33}}\epsilon_2 \qquad (2\text{-}5)$$

Applying the modified plane stress assumption to Eq (2-3), using the relation of Eq (2-5), and rearranging terms produces the lamina constitutive relation

$$\begin{Bmatrix}\sigma_1\\ \sigma_2\\ \sigma_6\\ \sigma_4\\ \sigma_5\end{Bmatrix} = \begin{bmatrix} Q_{11} & Q_{12} & 0 & 0 & 0 & 0\\ Q_{12} & Q_{22} & 0 & 0 & 0 & 0\\ 0 & 0 & Q_{66} & 0 & 0 & 0\\ 0 & 0 & 0 & Q_{44} & 0 & 0\\ 0 & 0 & 0 & 0 & Q_{55} & 0\end{bmatrix} \begin{Bmatrix}\epsilon_1\\ \epsilon_2\\ \epsilon_6\\ \epsilon_4\\ \epsilon_5\end{Bmatrix} \qquad (2\text{-}6)$$

where the Q_{ij} are reduced stiffness coefficients related to the C's by

$$Q_{ij}=C_{ij}-\frac{C_{i3}C_{j3}}{C_{33}} \qquad (2\text{-}7)$$

In terms of engineering coefficients,

$$Q_{11}=\frac{E_1}{\omega} \quad Q_{22}=\frac{E_2}{\omega} \quad Q_{12}=\frac{\nu_{21}E_2}{\omega}$$
$$Q_{66}=G_{12} \quad Q_{44}=G_{23} \quad Q_{55}=G_{13} \qquad (2\text{-}8)$$

where $\omega = 1- \nu_{12}\ \nu_{21}$.

Finally, in order to analyze a stack of plies, they must all be referenced to a global axis system and their effects summed:

$$\{\sigma_i\}_k=[T]\ [Q_{ij}]_k\ [T]^T\{\epsilon_i\}_k \qquad (2\text{-}9)$$

where

$$[T] = \begin{bmatrix} c^2 & s^2 & -2cs \\ s^2 & c^2 & 2cs \\ cs & -cs & c^2-s^2 \end{bmatrix} \quad for \quad \begin{bmatrix} Q_{11} & Q_{12} & 0 \\ Q_{12} & Q_{22} & 0 \\ 0 & 0 & Q_{66} \end{bmatrix}$$

$$[T] = \begin{bmatrix} c & -s \\ s & c \end{bmatrix} \quad for \quad \begin{bmatrix} Q_{44} & 0 \\ 0 & Q_{55} \end{bmatrix}$$

and c=cos(Φ), s=sin(Φ). With this transformation the constitutive relations are

$$\{\sigma_i\}_k = [\overline{Q}_{ij}]_k \ \{\epsilon_i\}_k \qquad (2\text{-}10)$$

with the transformed reduced stiffnesses

$$\overline{Q}_{11} = Q_{11}\cos^4\Phi + 2(Q_{12} + 2Q_{66})\sin^2\Phi\cos^2\Phi + Q_{22}\sin^4\Phi$$
$$\overline{Q}_{12} = (Q_{11} + Q_{22} - 4Q_{66})\sin^2\Phi\cos^2\Phi + Q_{12}(\sin^4\Phi + \cos^4\Phi)$$
$$\overline{Q}_{22} = Q_{11}\sin^4\Phi + 2(Q_{12} + 2Q_{66})\sin^2\Phi\cos^2\Phi + Q_{22}\cos^4\Phi$$

$$\overline{Q}_{16} = (Q_{11} - Q_{12} - 2Q_{66})\sin\Phi\cos^3\Phi + (Q_{12} - Q_{22} + 2Q_{66})\sin^3\Phi\cos\Phi$$
$$\overline{Q}_{26} = (Q_{11} - Q_{12} - 2Q_{66})\sin^3\Phi\cos\Phi + (Q_{12} - Q_{22} + 2Q_{66})\sin\Phi\cos^3\Phi$$
$$\overline{Q}_{66} = (Q_{11} + Q_{22} - 2Q_{12} - 2Q_{66})\sin^2\Phi\cos^2\Phi + Q_{66}(\sin^4\Phi + \cos^4\Phi)$$
$$\overline{Q}_{44} = Q_{44}\cos^2\Phi + Q_{55}\sin^2\Phi$$
$$\overline{Q}_{45} = (Q_{44} - Q_{55})\cos\Phi\sin\Phi$$
$$\overline{Q}_{55} = Q_{55}\cos^2\Phi + Q_{44}\sin^2\Phi$$

Strain Displacement Relations

The strain versus displacement relations in the SHELL code take into account the geometric nonlinearity arising from the panel's curvature. It is also within these relations that through the thickness shear effects are incorporated into the analysis. This development follows Dennis (8) who authored the original code.

The incorporation of transverse shear effects is accomplished by assuming a modified state of plane stress for the laminar (previously discussed) in which $\sigma_3=0$ (and hence $\epsilon_3=0$) but σ_4 and σ_5 are allowed to be small non-zero values. These transverse shear stresses are assumed to equal zero on the top and bottom surfaces of the shell, and the associated strains will vary parabolically through the shell thickness.

To start, one looks at the fully non-linear strain-displacement relations for an orthogonal curvilinear coordinate system taken from Saada (20) and presented below.

$$\begin{aligned}\gamma_{11} = & h_1\frac{\partial u_1}{\partial y_1}+\frac{h_1u_2}{h_2}\frac{\partial h_1}{\partial y_2}+\frac{h_1u_3}{h_3}\frac{\partial h_1}{\partial y_3}\\ & +\frac{1}{2}\left(\frac{\partial u_1}{\partial y_1}+\frac{u_2}{h_2}\frac{\partial h_1}{\partial y_2}+\frac{u_3}{h_3}\frac{\partial h_1}{\partial y_3}\right)^2\\ & +\frac{1}{2}\left(\frac{\partial u_2}{\partial y_1}-\frac{u_1}{h_2}\frac{\partial h_1}{\partial y_2}\right)^2+\frac{1}{2}\left(\frac{\partial u_3}{\partial y_1}-\frac{u_1}{h_3}\frac{\partial h_1}{\partial y_3}\right)^2\end{aligned} \qquad (2\text{-}11)$$

$$\gamma_{22}=h_2\frac{\partial u_2}{\partial y_2}+\frac{h_2u_3}{h_3}\frac{\partial h_2}{\partial y_3}+\frac{h_2u_1}{h_1}\frac{\partial h_2}{\partial y_1}$$
$$+\frac{1}{2}\left(\frac{\partial u_2}{\partial y_2}+\frac{u_3}{h_3}\frac{\partial h_2}{\partial y_3}+\frac{u_1}{h_1}\frac{\partial h_2}{\partial y_1}\right)^2 \qquad (2\text{-}12)$$
$$+\frac{1}{2}\left(\frac{\partial u_3}{\partial y_2}-\frac{u_2}{h_3}\frac{\partial h_2}{\partial y_3}\right)^2+\frac{1}{2}\left(\frac{\partial u_1}{\partial y_2}-\frac{u_2}{h_1}\frac{\partial h_2}{\partial y_1}\right)^2$$

$$\gamma_{33}=h_3\frac{\partial u_3}{\partial y_3}+\frac{h_3u_1}{h_1}\frac{\partial h_3}{\partial y_1}+\frac{h_3u_2}{h_2}\frac{\partial h_3}{\partial y_2}$$
$$+\frac{1}{2}\left(\frac{\partial u_3}{\partial y_3}+\frac{u_1}{h_1}\frac{\partial h_3}{\partial y_1}+\frac{u_2}{h_2}\frac{\partial h_3}{\partial y_2}\right)^2 \qquad (2\text{-}13)$$
$$+\frac{1}{2}\left(\frac{\partial u_1}{\partial y_3}-\frac{u_3}{h_1}\frac{\partial h_3}{\partial y_1}\right)^2+\frac{1}{2}\left(\frac{\partial u_2}{\partial y_3}-\frac{u_3}{h_2}\frac{\partial h_3}{\partial y_2}\right)^2$$

$$\gamma_{12}=\frac{1}{2}\left(h_1\frac{\partial u_1}{\partial y_2}+h_2\frac{\partial u_2}{\partial y_1}-u_2\frac{\partial h_2}{\partial y_1}-u_1\frac{\partial h_1}{\partial y_2}\right)$$
$$+\frac{1}{2}\left(\frac{\partial u_1}{\partial y_2}-\frac{u_2}{h_1}\frac{\partial h_2}{\partial y_1}\right)\left(\frac{\partial u_1}{\partial y_1}+\frac{u_2}{h_2}\frac{\partial h_1}{\partial y_2}+\frac{u_3}{h_3}\frac{\partial h_1}{\partial y_3}\right)$$
$$+\frac{1}{2}\left(\frac{\partial u_2}{\partial y_1}-\frac{u_1}{h_2}\frac{\partial h_1}{\partial y_2}\right)\left(\frac{\partial u_2}{\partial y_2}+\frac{u_1}{h_1}\frac{\partial h_2}{\partial y_1}+\frac{u_3}{h_3}\frac{\partial h_2}{\partial y_3}\right) \qquad (2\text{-}14)$$
$$+\frac{1}{2}\left(\frac{\partial u_3}{\partial y_1}-\frac{u_1}{h_3}\frac{\partial h_1}{\partial y_3}\right)\left(\frac{\partial u_3}{\partial y_2}-\frac{u_2}{h_3}\frac{\partial h_2}{\partial y_3}\right)$$

$$\gamma_{13}=\frac{1}{2}\left(h_3\frac{\partial u_3}{\partial y_1}+h_1\frac{\partial u_1}{\partial y_3}-u_1\frac{\partial h_1}{\partial y_3}-u_3\frac{\partial h_3}{\partial y_1}\right)$$
$$+\frac{1}{2}\left(\frac{\partial u_1}{\partial y_3}-\frac{u_3}{h_1}\frac{\partial h_3}{\partial y_1}\right)\left(\frac{\partial u_1}{\partial y_1}+\frac{u_3}{h_3}\frac{\partial h_1}{\partial y_3}+\frac{u_2}{h_2}\frac{\partial h_1}{\partial y_2}\right)$$
$$+\frac{1}{2}\left(\frac{\partial u_3}{\partial y_1}-\frac{u_1}{h_3}\frac{\partial h_1}{\partial y_3}\right)\left(\frac{\partial u_3}{\partial y_3}+\frac{u_1}{h_1}\frac{\partial h_3}{\partial y_1}+\frac{u_2}{h_2}\frac{\partial h_3}{\partial y_2}\right) \qquad (2\text{-}15)$$
$$+\frac{1}{2}\left(\frac{\partial u_2}{\partial y_1}-\frac{u_1}{h_2}\frac{\partial h_1}{\partial y_2}\right)\left(\frac{\partial u_2}{\partial y_3}-\frac{u_3}{h_2}\frac{\partial h_3}{\partial y_2}\right)$$

$$\gamma_{23}=\frac{1}{2}\left(h_3\frac{\partial u_3}{\partial y_2}+h_2\frac{\partial u_2}{\partial y_3}-u_2\frac{\partial h_2}{\partial y_3}-u_3\frac{\partial h_3}{\partial y_2}\right)$$
$$+\frac{1}{2}\left(\frac{\partial u_2}{\partial y_3}-\frac{u_3}{h_2}\frac{\partial h_3}{\partial y_2}\right)\left(\frac{\partial u_2}{\partial y_2}+\frac{u_3}{h_3}\frac{\partial h_2}{\partial y_3}+\frac{u_1}{h_1}\frac{\partial h_2}{\partial y_1}\right)$$
$$+\frac{1}{2}\left(\frac{\partial u_3}{\partial y_2}-\frac{u_2}{h_3}\frac{\partial h_2}{\partial y_3}\right)\left(\frac{\partial u_3}{\partial y_3}+\frac{u_2}{h_2}\frac{\partial h_3}{\partial y_2}+\frac{u_1}{h_1}\frac{\partial h_3}{\partial y_1}\right) \qquad (2\text{-}16)$$
$$+\frac{1}{2}\left(\frac{\partial u_1}{\partial y_2}-\frac{u_2}{h_1}\frac{\partial h_2}{\partial y_1}\right)\left(\frac{\partial u_1}{\partial y_3}-\frac{u_3}{h_1}\frac{\partial h_3}{\partial y_1}\right)$$

The u_i's are the displacements in the 1,2,and 3 directions respectively and the y_i's are the generalized coordinates in the 1,2, and 3 directions. The expressions for ϵ_{ij} are obtained by dividing the γ_{ij} by the product of the coordinate system scale factors h_ih_j. It is important to keep in mind the contracted notation discussed in Table 2-1. As stated earlier ϵ_3 is assumed to be zero and only the linear terms are kept for the transverse shear strains ϵ_4 and ϵ_5. Thus we see that (8):

$$\epsilon_4 = \frac{1}{h_2}\left[u_{3,2} + h_2 u_{3,3} - u_2 h_{2,3}\right]$$
$$\epsilon_5 = \frac{1}{h_1}\left[u_{3,1} + h_1 u_{1,3} - u_1 h_{1,3}\right] \qquad (2\text{-}17)$$

where the coordinate system scale factors for the cylindrical geometry used in this work are h_1=1, h_2=1- z/R, and h_3=1.

The displacement equations in the thickness variable z which permit the incorporation of the desired through the thickness features are (8):

$$u(x,\theta,z) = u^0 + z\psi_1 + z^2\phi_1 + z^3\gamma_1 + z^4\theta_1$$
$$v(x,\theta,z) = v^0\left[1-\frac{z}{R}\right] + z\psi_2 + z^2\phi_2 + z^3\gamma_2 + z^4\theta_2 \qquad (2\text{-}18)$$
$$w(x,\theta) = w$$

where u^0, v^0, w, ψ_i, ϕ_i, γ_i, and θ_i are functions of the coordinates x and θ. The displacements u^0 and v^0 are of the shell middle surface. The transverse displacement w is the same throughout the thickness since transverse normal strain is assumed negligible. The ψ_i terms are rotations of the surface normals in the x and s planes, and ϕ_i, γ_i, and θ_i are to be found by applying the assumptions that transverse shear stresses σ_4 and σ_5 are zero in the shell surfaces. Substituting the equations for v and w into Eq (2-17) for ϵ_4 yields (8):

$$\epsilon_4 = \frac{1}{1-\frac{z}{R}}\left[w_{,2} + (1-\frac{z}{R})\left(-\frac{v^0}{R} + \psi_2 + 2z\phi_2 + 3z^2\gamma_2 + 4z^3\theta_2\right)\right.$$
$$\left. + \frac{1}{R}\left(v^0(1-\frac{z}{R}) + z\psi_2 + z^2\phi_2 + z^3\gamma_2 + z^4\theta_2\right)\right] \qquad (2\text{-}19)$$

For zero transverse shear stress at the surfaces, the associated strain will also be zero. Enforcing this condition by substituting ±h/2 for z in Eq (2-19) and setting both resulting expressions to zero and hence equal to each other, one obtains by then solving for the unknown variables the following (8):

$$\phi_2 = 0$$
$$\theta_2 = \frac{\gamma_2}{2R} \qquad (2\text{-}20)$$
$$\left[1-\frac{h^2}{8R^2}\right] = -\frac{4}{3h^2}(\psi_2 + w_{,2})$$

Note that an h/R value of 1/5 (quite high for practical aerospace shell geometries) allows for the neglection of the h/R term in the left side of Eq (2-20). Replacing ϕ_2, θ_2 and γ_2 in Eq (2-19) with the results in Eq (2-20) one can find the transverse shear strain ϵ_4 in terms of transverse displacement w and rotation ψ_2 (8):

$$\epsilon_4 = \frac{1}{1-z/R}(w_{,2} + \psi_2)\left(1 - 4\frac{z^2}{h^2} + 8\frac{z^3}{3h^2R}\right) \qquad (2\text{-}21)$$

It should be noted that there are 1/R terms to be neglected. Therefore, the transverse shear strain-displacement relations, ϵ_4, along with a similar analysis with ϵ_5 (simpler since $h_1 = 1$), become (8):

$$\epsilon_4 = \frac{1}{1-z/R}(w_{,2} + \psi_2)\left(1 - 4\frac{z^2}{h^2}\right) \qquad (2\text{-}22a)$$

$$\epsilon_5 = (w_{,1} + \psi_1)\left(1 - 4\frac{z^2}{h^2}\right) \qquad (2\text{-}22b)$$

By replacing ϕ_2, θ_2 and γ_2 in Eq (2-18) it is found that the displacement equations are (8):

$$\begin{aligned} u(x,\theta,z) &= u^0 + z\psi_1 - \frac{4}{3h^3}z^3(\psi_1 + w_{,1}) \\ v(x,\theta,z) &= v^0\left[1-\frac{z}{R}\right] + z\psi_2 - \frac{4}{3h^2}z^3(\psi_2 + w_{,2}) \\ w(x,\theta) &= w \end{aligned} \qquad (2\text{-}23)$$

At this point, one can note that this formulation provides seven degrees of freedom: u; v; w; $w_{,1}$; $w_{,2}$; ψ_1 and ψ_2.

Now that the displacement equations which incorporate a parabolic through the thickness shear stress distribution have been developed, the in-plane kinematic equations are derived for the shell middle surface. The fully general

strain displacement relations are quite extensive; the theoretical development incorporating them can be found in Dennis' large displacement - moderate rotation general shell development (8). The general strain displacement relations of Eq (2-11) and (2-16) with the kinematics of Eq (2-23) will give the inplane shell strain displacement relations. These expressions can be specialized for a shell geometry of interest by defining the scale factors, h_i, using Eq (2-24) (8).

$$h_1 = \alpha_1(1 - z/R_1)$$
$$h_2 = \alpha_2(1 - z/R_2) \qquad (2\text{-}24)$$
$$h_3 = 1$$

where $\alpha_\gamma^2 = g_{\gamma\gamma}$ (no sum), which are called the metric coefficients for the orthogonal curvilinear coordinate system.

By substituting Eq (2-24) into Eq (2-11) - (2-16) and carrying out the indicated differentiation, one obtains for the inplane strain-displacement equations (8):

$$\epsilon_1 = \frac{\gamma_{11}}{h_1^2} = \epsilon_1^0 + z\chi_1^1 + z^2\chi_1^2 + z^3\chi_1^3 + z^4\chi_1^4 + z^6\chi_1^6 \qquad (2\text{-}25a)$$

$$\epsilon_2 = \frac{\gamma_{22}}{h_2^2} = \epsilon_2^0 + z\chi_2^1 + z^2\chi_2^2 + z^3\chi_2^3 + z^4\chi_2^4 + z^6\chi_2^6 \qquad (2\text{-}25b)$$

$$\epsilon_6 = \frac{2\gamma_{11}}{h_1 h_2} = \epsilon_6^0 + z\chi_6^1 + z^2\chi_6^2 + z^3\chi_6^3 + z^4\chi_6^4 + z^6\chi_6^6 \qquad (2\text{-}25c)$$

where the ϵ_j^o and the χ_j^i terms (j=1,2,6; i=1,2,3,4,6) are functions of the displacements and the scale factors, and can be found in Appendix A of (8). It is noted that the superscripts on the χ_j^i are not exponents. They are individual strain components that correspond to the power of z that multiplies it, and the subscripts on χ_j^i indicate the strain, ϵ_1, ϵ_2, or ϵ_6 that these components correspond with.

The following equivalent representation of the strains is conducive to the matrix operations of the potential energy formulation in the next section. The inplane strain displacement relations are represented by (8):

$$\epsilon_1 = \epsilon_1^0 + z^p \chi_{1p} \; ; \quad (p=1,..,7)$$

where

$$\epsilon_1^0 = u_{,1} + \frac{1}{2}(u_{,1}^2 + v_{,1}^2 + w_{,1}^2) \tag{2-26a}$$

$$\epsilon_2 = \epsilon_2^0 + z^p \chi_{2p} \; ; \quad (p=1,..,7)$$

where

$$\epsilon_2^0 = v_{,2} - \frac{w}{R} + \frac{1}{2}(u_{,2}^2 + v_{,2}^2 + w_{,2}^2 + \frac{v^2}{R^2} + \frac{w^2}{R^2}) + \frac{vw_{,2}}{R} - \frac{v_{,2}w}{R} \tag{2-26b}$$

$$\epsilon_6 = \epsilon_6^0 + z^p \chi_{6p} \; ; \quad (p=1,..,7)$$

where

$$\epsilon_6^0 = u_{,2} + v_{,1} + u_{,1}u_{,2} + v_{,1}v_{,2} + w_{,1}w_{,2} + \frac{1}{R}(vw_{,1} - v_{,1}w) \tag{2-26c}$$

Note: The higher order bending strain-displacement relations, χ_{ip} (i=1,2,6; p=1,..,7), are completely shown in (8).

The transverse shear strains (in similar form) are (8):

$$\epsilon_4 = \epsilon_4^0 + z^p \chi_{4p} \; ; \quad \begin{matrix} \epsilon_4^0 = w_{,2} + \psi_2 \\ \chi_{42} = 3k(w_{,2} + \psi_2) \\ \chi_{4p}(p=1,3,4,5,6,7) = 0 \end{matrix} \tag{2-27a}$$

$$\epsilon_5 = \epsilon_5^0 + z^p \chi_{5p} \; ; \qquad \begin{matrix} \epsilon_5^0 = w_{,1} + \psi_1 \\ \chi_{52} = 3k(w_{,1} + \psi_1) \\ \chi_{5p}(p=1,3,4,5,6,7) = 0 \end{matrix} \tag{2-27b}$$

This allows assembly of the strain displacement equations into a matrix format:

$$\begin{Bmatrix} \epsilon_1 \\ \epsilon_2 \\ \epsilon_3 \end{Bmatrix} = \begin{Bmatrix} \epsilon_1^0 \\ \epsilon_2^0 \\ \epsilon_3^0 \end{Bmatrix} + \begin{bmatrix} \chi_{11} & \chi_{12} & \chi_{13} & \chi_{14} & \chi_{15} & \chi_{16} & \chi_{17} \\ \chi_{21} & \chi_{22} & \chi_{23} & \chi_{24} & \chi_{25} & \chi_{26} & \chi_{27} \\ \chi_{61} & \chi_{62} & \chi_{63} & \chi_{64} & \chi_{65} & \chi_{66} & \chi_{67} \end{bmatrix} \begin{Bmatrix} z \\ z^2 \\ z^3 \\ z^4 \\ z^5 \\ z^6 \\ z^7 \end{Bmatrix} \tag{2-28}$$

$$\begin{Bmatrix} \epsilon_4 \\ \epsilon_5 \end{Bmatrix} = \begin{Bmatrix} \epsilon_4^0 \\ \epsilon_5^0 \end{Bmatrix} + \begin{bmatrix} \chi_{42} \\ \chi_{52} \end{bmatrix}$$

In a general expression,

$$\{\mathcal{E}\} = \{\mathcal{E}^0\} + [X]\{Z\} \tag{2-29}$$

It is worth noting that these kinematics avoid the common pitfall of shear locking, wherein the model becomes artificially stiff as the shell thickness is decreased. This is a problem with finite element formulations which incorporate constant or linearly distributed shear strain through the thickness, and it necessitates the use of a correction factor. However, examination of the compatibility relations associated with the strain

displacement equations developed in this section shows that the terms associated with transverse shear drop out as thickness is reduced to zero (8).

Note the kinematics developed in this section are specifically for the cylindrical geometry. The analysis accomplished for this work uses these large displacement - moderate rotation formulations.

Potential Energy

The shell potential energy is the sum of the internal strain energy and the work done by external forces:

$$\prod_p = E + W \tag{2-30}$$

where the internal strain energy is given by

$$E = \int_\Omega \int_h \frac{1}{2}([\bar{Q}]\{\mathscr{E}\})\, dz\, d\Omega \tag{2-31}$$

where Ω represents the shell middle surface. The internal strain energy E is composed of in-plane and normal terms (set E_1) and transverse shear terms (set E_2). Expanding the expression for E by inserting Eqs (2-27) through (2-29) into Eq (2-31) gives

$$E_1 = \frac{1}{2}\int_\Omega\int_h \left[\bar{Q}_{11}(\epsilon_1^0+z^p\chi_{1p})^2 + \bar{Q}_{22}(\epsilon_2^0+z^p\chi_{2p})^2 + 2\bar{Q}_{12}(\epsilon_1^0+z^p\chi_{1p})(\epsilon_2^0+z^r\chi_{2r}) + \bar{Q}_{66}(\epsilon_6^0+z^p\chi_{6p})^2 + 2\bar{Q}_{16}(\epsilon_1^0+z^p\chi_{1p})(\epsilon_6^0+z^r\chi_{6r}) + 2\bar{Q}_{26}(\epsilon_2^0+z^p\chi_{2p})(\epsilon_6^0+z^r\chi_{6r})\right] dz\, d\Omega \quad (2\text{-}32)$$

$$E_2 = \frac{1}{2}\int_\Omega\int_h \left[\bar{Q}_{44}(\epsilon_4^0+z^2\chi_{42})^2 + \bar{Q}_{55}(\epsilon_5^0+z^p\chi_{52})^2 + 2\bar{Q}_{45}(\epsilon_4^0+z^2\chi_{42})(\epsilon_5^0+z^2\chi_{52})\right] dz\, d\Omega \quad (2\text{-}33)$$

where p,r=1,2,...,7. Integrating the z over ± h/2 yields the equation for strain energy as a function of the middle surface only, which is the desired formulation for this problem. A further simplification performed in the development of the SHELL program is one of symmetry in ply layup. This results in the cancellation of elasticity arrays which are multiplied by odd powers of the transverse coordinate z. Rearranging yields the final forms of

$$E_1 = \frac{1}{2}\int_\Omega \{\mathscr{E}^0\}^T[A]\{\mathscr{E}^0\}\, d\Omega \quad (2\text{-}34)$$

$$E_2 = \frac{1}{2}\int_{\Omega}(\{\mathscr{E}^0\}^T[A]\{\mathscr{E}^0\} + 2\{\mathscr{E}^0\}^T[D]\,[\mathbf{X}] + [\mathbf{X}]^T[F]\,[\mathbf{X}])\, d\Omega \qquad (2\text{-}35)$$

where stiffness matrices $\{[A,D,F]\} = \int_h [Q]\ \{1,\ z^2,\ z^4\}\ dz$.

The 36 DOF Element

The SHELL computer code uses a 36 DOF element developed by Dennis (8) and pictured in Fig (2-3). The seven degrees of freedom at each corner node were found in the previous section to be u, v, w, $w_{,1}$, $w_{,2}$, γ_1 and γ_2. The mid-side nodes have only the two inplane degrees of freedom u and v. C^0 continuity is required of all but w and its derivatives which require C^1 continuity. Lagrangian bilinear interpolation is used for u, v, γ_1 and γ_2 and non conforming Hermitian interpolation is used for w, $w_{,1}$ and $w_{,2}$.

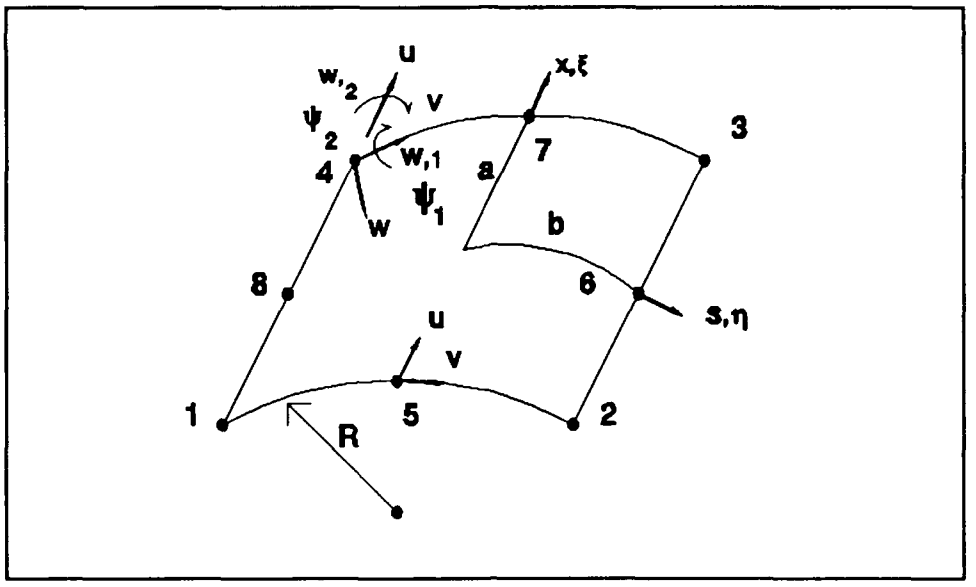

Figure 2-3. SHELL 36 Degree of Freedom Element

The assumed transverse displacement equation for the cylindrical shell element is

$$w(x,s)=a_1 + a_2x + a_3s + a_4x^2 + a_5xs + a_6s^2 + a_7x^3 + a_8x^2s + a_9xs^2 + a_{10}s^3 + a_{11}x^3s + a_{12}xs^3 \qquad (2\text{-}36)$$

This rectangular element may be isoparametrically scaled and oriented such that the longitudinal coordinate $x \rightarrow \xi$, the circumferential coordinate $s \rightarrow \eta$, and the side lengths are scaled by

$$\xi = \frac{x}{a} \qquad \eta = \frac{s}{b} \qquad (2\text{-}37)$$

where a and b are the scaled element half dimensions in the ξ and η directions respectively. Now the element transverse displacement equation can be written as:

$$w(x,s) = [\chi_1\ \chi_2\ \chi_3\ \chi_4] \begin{Bmatrix} q_1 \\ q_2 \\ q_3 \\ q_4 \end{Bmatrix} \tag{2-38}$$

where $\{q\}_k^T = \{w\ w_{,1}\ w_{,2}\}$ for the kth corner node, and the χ_i's are Hermitian shape functions (6):

$$\chi_k^T = \begin{Bmatrix} \chi_{k1} \\ \chi_{k2} \\ \chi_{k3} \end{Bmatrix} = \begin{Bmatrix} \frac{1}{8}(1+\xi_k\xi)(1+\eta_k\eta) \\ \qquad (2+\xi_k\xi+\eta_k\eta-\xi^2-\eta^2) \\ \frac{a}{8}\xi_k(1+\xi_k\xi)^2(\xi_k\xi-1)(1+\eta_k\eta) \\ \frac{b}{8}\eta_k(1+\xi_k\xi)(\eta_k\eta-1)(1+\eta_k\eta)^2 \end{Bmatrix} \tag{2-39}$$

The formulations for DOF's u, v and ψ_i is a simple Lagrangian form, and the midside nodes 5-8 are also included:

$$\begin{Bmatrix} u \\ v \\ \psi_1 \\ \psi_2 \end{Bmatrix} = \begin{bmatrix} Q_1 & 0 & 0 & 0 & \dots & Q_4 & 0 & 0 & 0 & Q_5 & \dots & Q_8 \\ 0 & Q_1 & 0 & 0 & \dots & 0 & Q_4 & 0 & 0 & 0 & \dots & 0 \\ 0 & 0 & N_1 & 0 & \dots & 0 & 0 & N_4 & 0 & 0 & \dots & 0 \\ 0 & 0 & 0 & N_1 & \dots & 0 & 0 & 0 & N_4 & 0 & \dots & 0 \end{bmatrix} \begin{Bmatrix} q_1 \\ q_2 \\ q_3 \\ q_4 \\ q_5 \\ q_6 \\ q_7 \\ q_8 \end{Bmatrix}$$

where $\{q\}_k^T=\{u\ v\ \psi_1\ \psi_2\}$ for nodes 1 through 4 and {u v} for nodes 5 through 8, and N and Q are linear and quadratic (respectively) Lagrangian shape functions (6):

$$N_k = \frac{1}{4}(1+\xi_k\xi)(1+\eta_k\eta)$$

$$Q_k=\frac{1}{4}(1+\xi_k\xi)(1+\eta_k\eta)(\xi_k\xi+\eta_k\eta-1),$$

$$k=1,2,3,4 \qquad (2\text{-}40)$$

$$Q_k=\frac{1}{2}(1-\xi^2)(1+\eta_k\eta),\ k=6,8$$

$$Q_k=\frac{1}{2}(1-\eta^2)(1+\xi_k\xi),\ k=5,7$$

The overall equation defining the isoparametric discretization of continuum displacements into nodal displacements is obtained by merging the above relationships:

$$\underset{(7x1)}{|u|} = \underset{(7x36)}{[N]}\ \underset{(36x1)}{\{q\}} \qquad (2\text{-}41)$$

Static Finite Element Solution

The solution to the static finite element problem involves finding the equilibrium state between applied load and structural response. This state can be determined by finding where the variation of the system potential energy is zero. Recall Eq (2-30):

$$\Pi_p = E + W \tag{2-30}$$

where now internal strain energy can be represented by

$$E = \frac{1}{3} q^T \left[K + \frac{N_1}{2} + \frac{N_2}{3} \right] q = \frac{1}{2} q^T \bar{K} q \tag{2-42}$$

where q is a column array of nodal displacements, K includes the constant stiffness terms, N_1 includes the stiffness terms linear in displacement and N_2 includes the terms quadratic in displacement. The external work can be represented as

$$W = -q^T \lambda P \tag{2-43}$$

where P is a column vector of applied nodal loads and λ is a multiplier which will be discussed in the next section on the static solution algorithm. Equilibrium is defined as the state at which internal strain energy and external work balance, thus potential energy will be at a relative minimum. This point can be found by substituting Eqs (2-42) and (2-43) into Eq (2-30) and taking the first variation:

$$\delta \Pi_p = \delta q^T [\bar{K} q - \lambda p] = 0 \tag{2-44}$$

Since displacements δq are nonzero for all but the trivial

solution, the bracketed expression must be zero for equilibrium. It is a function (called f) of q and λ:

$$\overline{K}\,q - \lambda p = 0 = f(q,\lambda) \qquad (2\text{-}45)$$

Since K varies with load and displacement, a numerical ıterative solution is used to solve Eq (2-45) incorporating the Newton-Raphson method.

Static Solution Algorithm

For static analysis, the SHELL code uses the solution technique advanced by Riks (18,19) and Wempner (27) and demonstrated by Crisfield (7) of incrementing a desired arc length along the load-displacement curve while solving iteratively via the Newton-Raphson method. Called the modified Riks-Wempner method, and added to the SHELL code by Tsai and Palazotto (26), this allows for tracing of the load displacement response through both load reversing (snap through) and displacement reversing (snap back) critical points, so the most complex behavior can be continuously followed.

The essence of the Riks-Wempner method is that neither load P nor displacement q is independently controlled; rather a selected "arc" length Δs (actually the chord) of the load-displacement curve is incremented. The equilibrium condition is found which satisfies the relation:

$$\Delta q_{i+1} \cdot \Delta q_{i+1} + \Delta \lambda_{i+1}^2 \, P \cdot P = \Delta s^2 \qquad (2\text{-}46)$$

where Δ_{i+1} is the incremental displacement for step i+1, and $\Delta\lambda_{i+1}$ is the fraction of load P applied at step i+1. The effect of the constraint equation (2-46) is that each subsequent step solution is searched for on an arc of radius Δs from the current solution. The initial value for the quantity $\Delta\lambda$ is specified with the problem input data.

To apply the Newton-Raphson method, the first variation of Eq (2-45) is taken and applied at step i:

$$K_T \, \delta q_i = \delta \lambda_i P - f(q_i, \lambda_i) \qquad (2\text{-}47)$$

where

$$\delta q_i = \delta q_{i1} + \delta \lambda_i \delta q_{i2} \qquad (2\text{-}47a)$$

the out-of-balance term is

$$\delta q_{i1} = -K_T^{-1} \, f(q_i, \lambda_i) \qquad (2\text{-}47b)$$

the linear term is

$$\delta q_{i2} = K_T^{-1} \, P \qquad (2\text{-}47c)$$

and

$$K_T = [K + N_1 + N_2] \qquad (2\text{-}47d)$$

The following briefly describes the operation of the algorithm on load step n, i denotes an iteration at step n along the solution path, and Fig 2-4 provides a simplified illustration of the algorithm.

a.) The tangent stiffness matrix K_T at the current deformed geometry is determined.

b.) The linear incremental displacement δ_{i2} is computed (Eq 2-47c).

c.) The first iteration computes $\Delta q_1 = \Delta\lambda_1\delta_{i2}$, with $\Delta\lambda_1=\Delta\lambda_{n-1}$, or a user defined value if n=1 (first increment). The parameter $\Delta\lambda$ indicates the fraction of total load to be applied at the first increment.

d.) The constraint equation (2-46) is solved for Δs. The load term is often ignored in this relation, since the load and displacement values typically differ by many orders of magnitude, which can cause numerical difficulty. Convergence to a solution is not hindered by ignoring load at this step.

e.) K_T is updated at $q = q_n + \Delta q_i$.

f.) The out-of-balance displacement δ_{i1} is computed (Eq 2-47b).

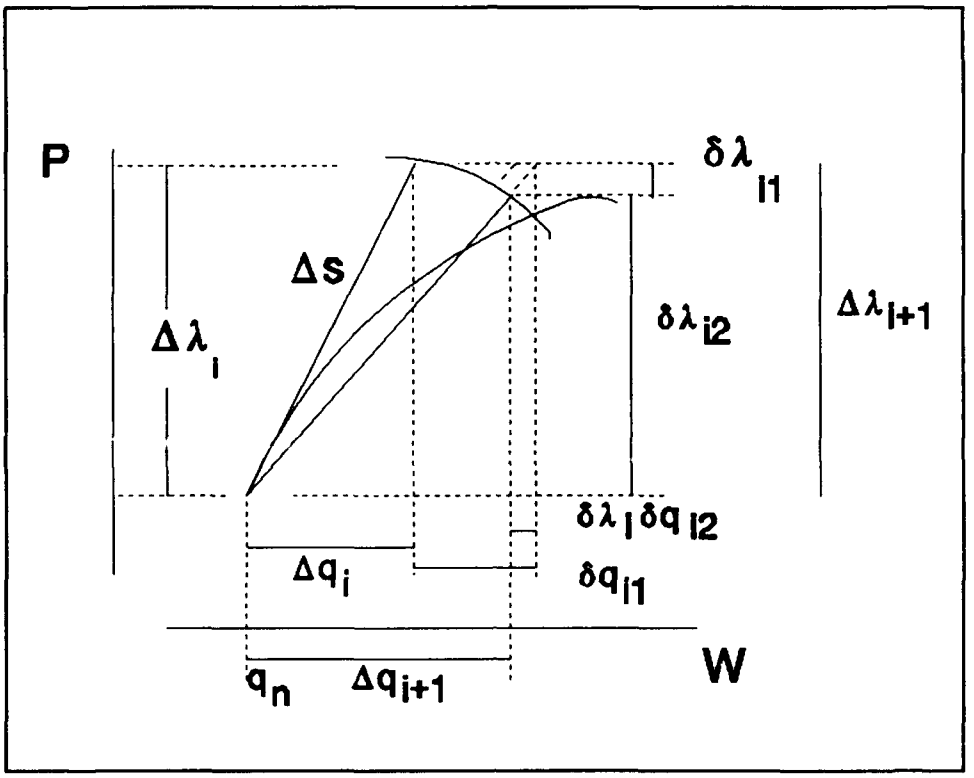

Figure 2-4. Riks Method Solution Step

g.) Eqs (2-47a) in (2-46) are solved for $\delta\lambda_i$, which will have two roots $\delta\lambda_{i1}$ and $\delta\lambda_{i2}$ due to the quadratic feature.

h.) $\delta\lambda_i$ is selected from $\delta\lambda_{i1}$ and $\delta\lambda_{i2}$, by criteria detailed in Crisfield (7), to ensure that the solution path does not return to equilibrium points previously obtained.

i.) Displacement increment $\Delta q_{i+1} = \Delta q_i + \delta q_i$ and load factor increment $\Delta\lambda_{i+1} = \Delta\lambda_i + \delta\lambda_i$ are updated.

j.) When Δq_i and $\Delta \lambda_i$ computed on successive iteration (steps e-i) differ by less than a selected convergence tolerance, the step n solution has been found:

$$\begin{aligned} \Delta q_i &\rightarrow \Delta q_n \\ \Delta \lambda_i &\rightarrow \Delta \lambda_n \end{aligned} \tag{2-48}$$

At the completion of each step, cumulative displacement and load factors are computed:

$$\begin{aligned} q_n &= q_{n-1} + \Delta q_n \\ \lambda_n &= \lambda_{n-1} + \Delta \lambda_n \end{aligned} \tag{2-49}$$

This technique can follow an equilibrium path which progresses in any direction, by solving for negative incremental displacement or load, or both. This allows one to automatically solve for even the most convoluted nonlinear equilibrium curve, without concern for the singularities at critical load or displacement points.

The efficiency of the algorithm is improved by scaling the step (n+1)'s target Δs length by the ratio of a user selected desired number of iterations to the number of iterations to converge to step n. Thus, in near-linear parts of the load displacement curve, wide spacing of solution points is allowed; when the curve rounds corners

(around limit points) the method has to iterate more to converge and hence Δs is reduced until the curve straightens out again.

The inability to solve for equilibrium at a limit load point (as occurs in other techniques) is circumvented due to the nature of the stepping method. The technique shoots a tangent from the current equilibrium point, then searches an arc about the tip for the next solution point, so the exact limit load point is almost always skipped over. Auxiliary equations can be programmed to enable a more exact determination of the critical point (18).

Dynamic Equations of Motion

Tsai and Palazotto (14) have extended the SHELL code for the study of nonlinear vibration in cylindrical shells. The equations of motion for the cylindrical shell are derived via Hamilton's principal where the variation in the time integral of total energy is set to zero:

$$\delta \int_{t_1}^{t_2} (E-T-W_e) = 0 \qquad (2\text{-}50)$$

where E is the potential strain energy, T is the kinetic energy and W_e is the work of the external forces.

The variational components δE, δT, and δW_e for a laminated plate or shell are given by:

$$\delta E=\int_{\Omega} \sum_{k=1}^{L} \int_{\zeta_{k-1}}^{\zeta_k} \{\sigma_{ij}^{(k)} \delta e_{ij}^{(k)} + c^{(k)} v_j^{(k)} \delta u_j^{(k)} + P_j^{(k)} \delta u_j^{(k)}\} \, d\zeta d\Omega \tag{2-51}$$

and

$$\delta T = \int_{\Omega} \sum_{k=1}^{L} \int_{\zeta_{k-1}}^{\zeta_k} \{\rho^{(k)} v_j^{(k)} \delta v_j^{(k)}\} \, d\zeta d\Omega \tag{2-52}$$

and

$$\delta W_e = \int_{\Omega} F_j \delta u_j \, d\Omega \tag{2-53}$$

where i,j=1,2,3, ζ_{k-1} and ζ_k are positions at the bottom and top surface of the k-th layer, Ω is the domain of the neutral surface, $\sigma_{ij}^{(k)}$, $\delta\epsilon_{ij}^{(k)}$, $P_j^{(k)}$, $\delta u_j^{(k)}$, $v_j^{(k)}$, $\rho^{(k)}$, $c^{(k)}$, are stress tensor, virtual strain tensor, body force vector, virtual displacement vector, velocity vector, mass density, damping coefficient for the k-th layer, and F_j is the external force vector respectively, L is the total number of layers in a laminated shell.

From Eq (2-50), the finite element formulation is derived:

$$MU^{(2)} + CU^{(1)} + K(U^{(0)})U^{(0)} = F(t) \tag{2-54}$$

where K is the stiffness matrix for large displacement/rotation of cylindrical shells which was derived earlier and presented again in slightly different form:

$$K(U^{(0)}) = K_0 + \frac{K_1(U^{(0)})}{2} + \frac{K_2(U^{(0)})}{3} \qquad (2\text{-}55)$$

where $U^{(0)}$, $U^{(1)}$, $U^{(2)}$ are the displacement, velocity, and acceleration vectors at each nodal point, K_0 is a constant stiffness matrix, K_1 is a stiffness matrix related to linear displacement, K_2 is a stiffness matrix related to quadratic displacement, and P(t) is the external load applied at each node. The consistent mass matrix is obtained as described in reference (14) by substituting Eq (2-41) into Eq (2-52)

$$M = \int_{\Omega} \sum_{k=1}^{L} \int_{\zeta_{k-1}}^{\zeta} \rho^{(k)} [N]^T [R]^T [R] [N] \, d\zeta d\Omega \qquad (2\text{-}56)$$

where [N] is the overall matrix of shape functions described in Eqs (2-39) and (2-40) and [R] is a matrix containing coordinate system scale factors as shown below:

$$[R] = \begin{bmatrix} 1 & 0 & 0 & k\zeta^3 & 0 & k\zeta^3+\zeta & 0 \\ 0 & 1-\frac{\zeta}{R} & 0 & 0 & k\zeta^3 & 0 & k\zeta^3+\zeta \\ 0 & 0 & 1 & 0 & 0 & 0 & 0 \end{bmatrix}$$

where $k = -4/3h^2$, h is the shell thickness, R is the radius of the shell and ζ is the position along the z axis or the surface normal. The damping matrix is obtained in a similar manner.

$$C = \int_{\Omega} \sum_{k=1}^{L} \int_{\zeta_{k-1}}^{\zeta_k} c^{(k)} [N]^T [R]^T [R] [N] \, d\zeta d\Omega \qquad (2\text{-}57)$$

Solution Technique for Dynamic Problems

To solve the nonlinear dynamic problem SHELL uses the beta-m method which is a generalization of Newmark's time marching integration scheme. It provides a general single step algorithm applicable to initial value problems and is specialized by specifying the method order m along with m integration parameters, $\beta_0, \beta_1, \beta_2, \ldots \beta_{m-1}$. For a particular choice of m, the integration parameters provide a subfamily of methods which control accuracy and stability. The finite difference scheme is not required in this method. This provides a better way for computer programming than the regular methods such as Newmark's method. The beta-m method is defined by

$$U_{n+1}^{(k)} = q_k + b_k \Delta U^{(m)} \qquad (2\text{-}58)$$

where

$$q_k = \sum_{j=k}^{m} \frac{U_n^{(j)} h^{j-k}}{(j-k)!} \tag{2-59}$$

and

$$b_k = \frac{\beta_k h^{m-k}}{(m-k)!} \tag{2-60}$$

and k=0,1,...,m, β_m is defined to be equal one, and h is the time increment for each time step. The method order m implies that $U_n^{(m)}$ is the highest derivative to be retained (m=2 is Newmark). For this research m=2 for all analysis. Also, throughout this work, β_0= 0.5, β_1=0.5 and β_1=1.0 as suggested by Hatona and Zienkiewicz (12) for an unconditionally stable analysis. Substituting Eq (2-58) into Eq (2-54) at time t_{n+1}, results in

$$\begin{aligned} &\left[b_2 M + b_1 C + b_0 K(q_0 + \Delta U^{(m)})\right] \Delta U^{(m)} = \\ &\quad P_{n+1} - \{M q_2 + C q_1 + K(q_0 + b_0 \Delta U^{(m)})\, q_0\} \end{aligned} \tag{2-61}$$

where P_{n+1} is the applied load at time t_{n+1}, b_0, b_1, b_2, are scalers dependent on the integration parameters as shown in Eq (2-60), and q_0, q_1, q_2 are history vectors known at time t_n as shown in Eq (2-59). Eq (2-61) results in a set of nonlinear algebraic equations. The Newton-Raphson iterative

method is adopted here to solve Eq (2-61). At each time step the following assumption is made

$$\Delta U_{i+1}^{(m)} = \Delta U_i^{(m)} + \delta U_i^{(m)} \tag{2-62}$$

where i is the iteration number. Applying the Newton-Raphson method to Eq (2-61) and using Eq (2-62) yields

$$\begin{aligned}\left[b_2 M + b_1 C + b_0 K_T(q_0 + b_0 \Delta U_i^{(m)}\right] \delta U_i = \\ P_{n+1} - M\left\{q_2 + b_2 \Delta U_i^{(m)}\right\} - C\left\{q_1 + b_1 \Delta U_i^{(m)}\right\} \\ - K\left(q_0 + b_0 \Delta U_i^{(m)}\right)\left\{q_0 + b_0 \Delta U_i^{(m)}\right\}\end{aligned} \tag{2-63}$$

where K_T is the updated tangential stiffness matrix.
Eq (2-63) is then solved by the following algorithm:

1.) Given $U_n^{(0)}$, $U_n^{(1)}$,....,$U_n^{(m)}$, at time t_n, the solution at time t_{n+1} is desired.

2.) $q_0, q_1, \ldots, q_m$, are calculated from Eq (2-59).

3.) Given $\Delta U_i^{(m)}$ and $U_{n+1}^{(m)}$ from the i-th iteration, the right-hand side of Eq (2-63) is obtained along with the updated tangential stiffness matrix.

4.) Eq (2-63) is used to solve for the primary unknown, $\delta U_i^{(m)}$.

5.) The update of the solution vector $\Delta U_{i+1}^{(m)}$ is calculated from Eq (2-62).

6.) $U_{n+1}^{(0)}$, $U_{n+1}^{(1)}$,....,$U_{n+1}^{(m)}$ is updated for the i+1-th iteration from Eq (2-58).

7.) If

$$\frac{\left\{\sqrt{\sum_{I=1}^{L}(U_{n+1}^{(0)})_1^2}\right\}_{i+1} - \left\{\sqrt{\sum_{I=1}^{L}(U_{n+1}^{(0)})_1^2}\right\}_{i}}{\left\{\sqrt{\sum_{I=1}^{N}(U_{n+1}^{(0)})_1^2}\right\}_{i}} \leq \epsilon \qquad (2\text{-}64)$$

then the algorithm goes back to step (1) for the next time step, otherwise, it goes to step (3) for the next iteration. 1 is the degree of freedom number and L is the total number of dof's in the finite element model, ϵ is the given convergence criterion.

The above procedures are terminated when t_n is equal to the given time duration.

III. RESULTS/DISCUSSION

This section presents results of analysis done on various problems to further evaluate the nonlinear dynamic response of a composite cylindrical panel. A static snap-through analysis was accomplished on an isotropic arch using the Riks technique and compared to an analysis done by Dennis (8) using a displacement control method. Also, a static analysis of an arch is compared to work by Belytschko and Glaum (3). Then the dynamic response of an isotropic panel is compared to some present results by Clough and Wilson (5). Finally, the majority of work presented shows both a laminated composite arch and shell subjected to a pre-buckling and a post-buckling load and the time dependent behavior compared to a static analysis.

It should be noted that all finite element analysis done in this research took advantage of using 1/4 panel symmetry in order to reduce the number of elements and refine the mesh size. The acceptability of using symmetry with the SHELL code is discussed in reference (23) by Silva.

Simple Supported Isotropic Arch

A static snap-through analysis of a simple supported circular arch was accomplished where the geometrical and material quantities are shown below.

E = 10.0E6 psi

ν = 0

R = 100 in. (radius)

h = 1.0 in. (thickness)

w = 1.0 in. (width)

θ = 53.13 deg

The mesh incorporated 46 identical elements modeling 1/4 of the arch with an aspect ratio of approximately four to one as shown in Figs (3-1) and (3-2).

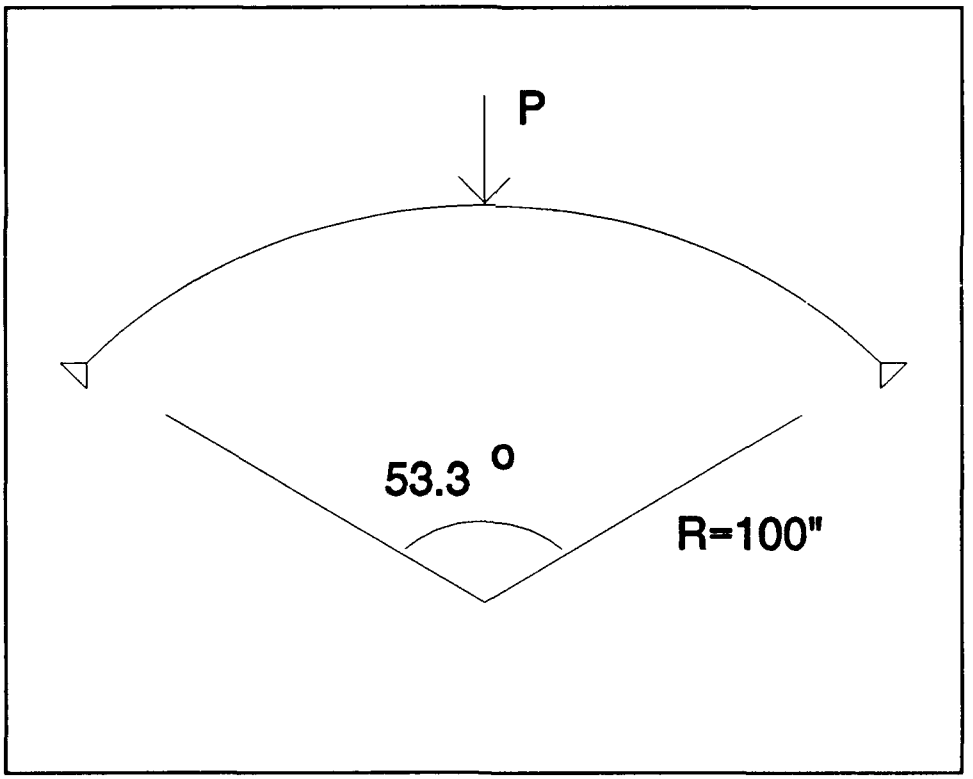

Figure 3-1. Simple Supported Isotropic Arch

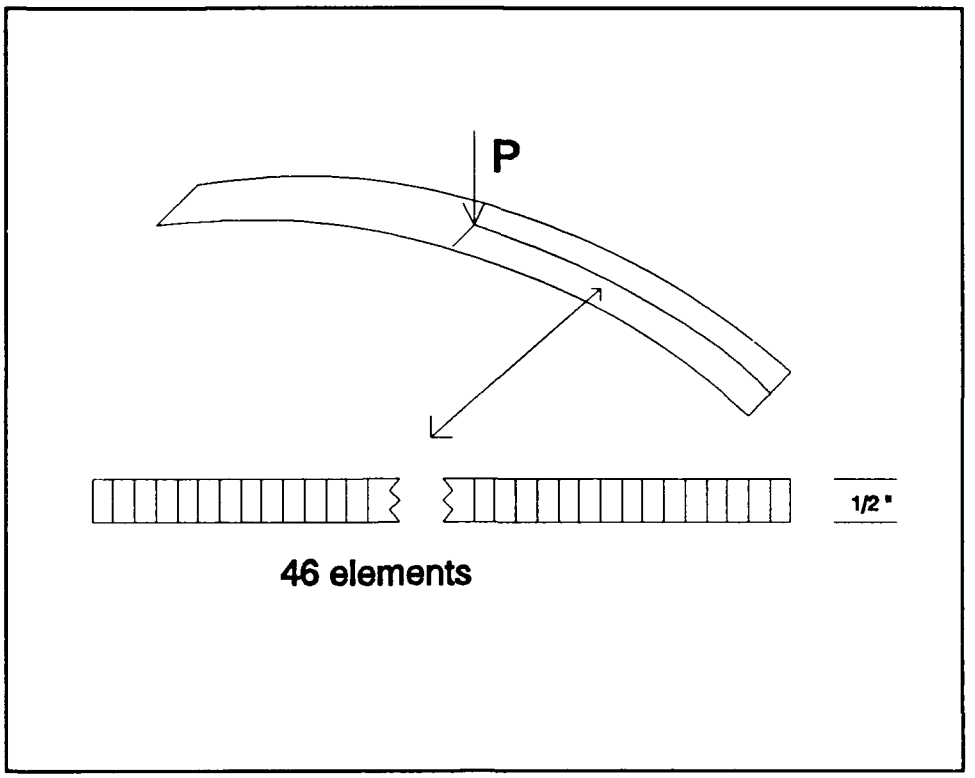

Figure 3-2. Mesh for Isotropic Arch

The loading is applied radially inward exactly at the center of the arch. This results in a symmetric response where the center of the arch displaces only radially. The solution by Dennis (8) was obtained by incrementing components of displacement and Fig 3-3 shows a comparison of the center load displacement of the arch.

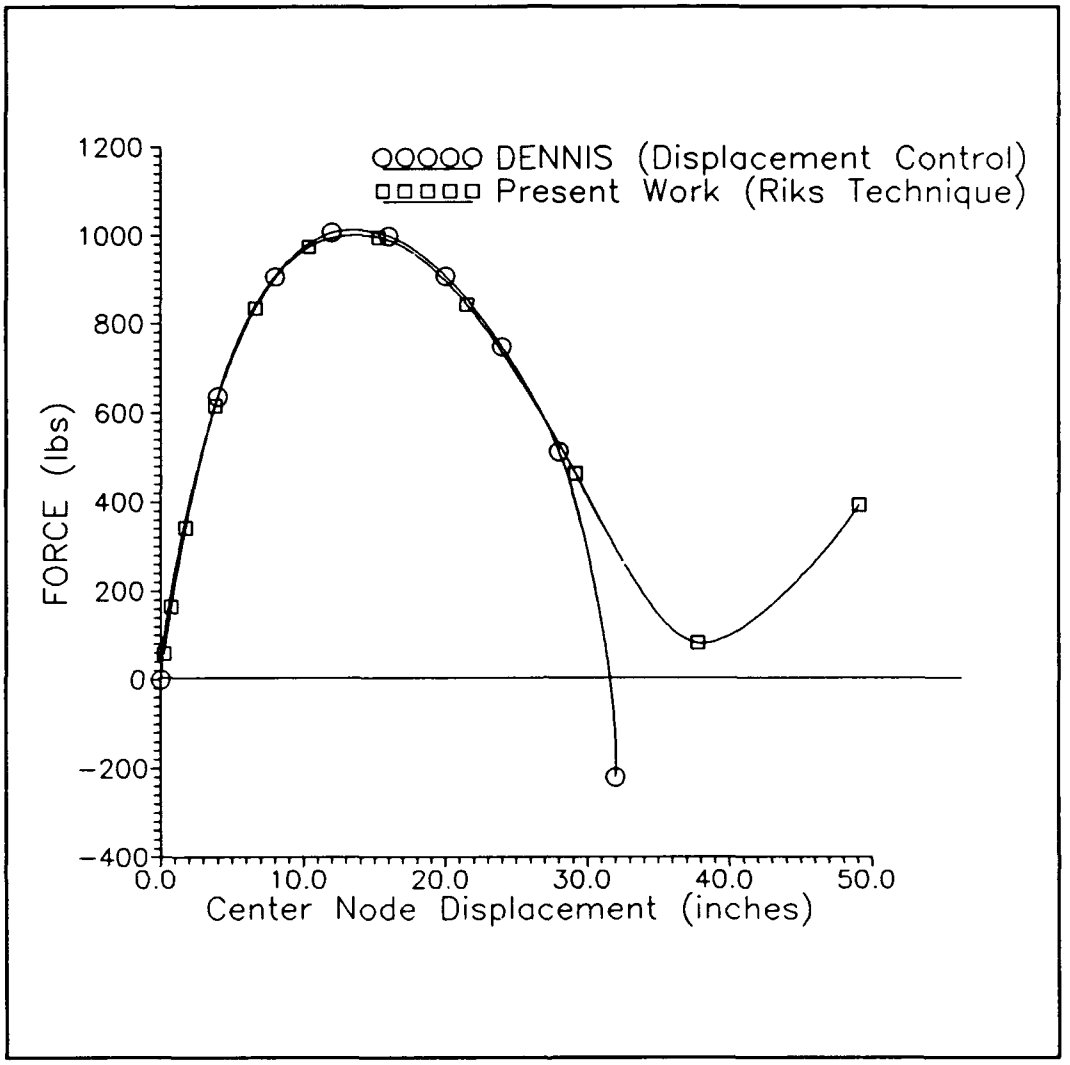

Figure 3-3. Force vs Displacement of Center Node, Simply Supported Isotropic Arch

As can be seen, both analyses predict the same pre-buckling load-displacement curve but the Riks algorithm allows for a tracing of the equilibrium path to a new post-buckling solution. The Riks method steps past singular areas and allows uninterrupted tracing of the equilibrium path.

Clamped Isotropic Arch

A static collapse analysis of a clamped arch was accomplished and compared to work done by Belytschko and Glaum (3). Geometric and material quantities are:

E = 10.0E6 psi	h = 0.1875 in
ν = 0	w = 1.0 in
R = 113.114 in.	θ = 17.22 deg

The solution uses the fully nonlinear strain-displacement relations of the SHELL code. Mesh sizes of 10 and 20 elements were used with almost identical results thus convergence is assumed. Belytschko and Glaum reach convergence for their fully modeled arch when the mesh size is decreased from 16 to 32 elements.

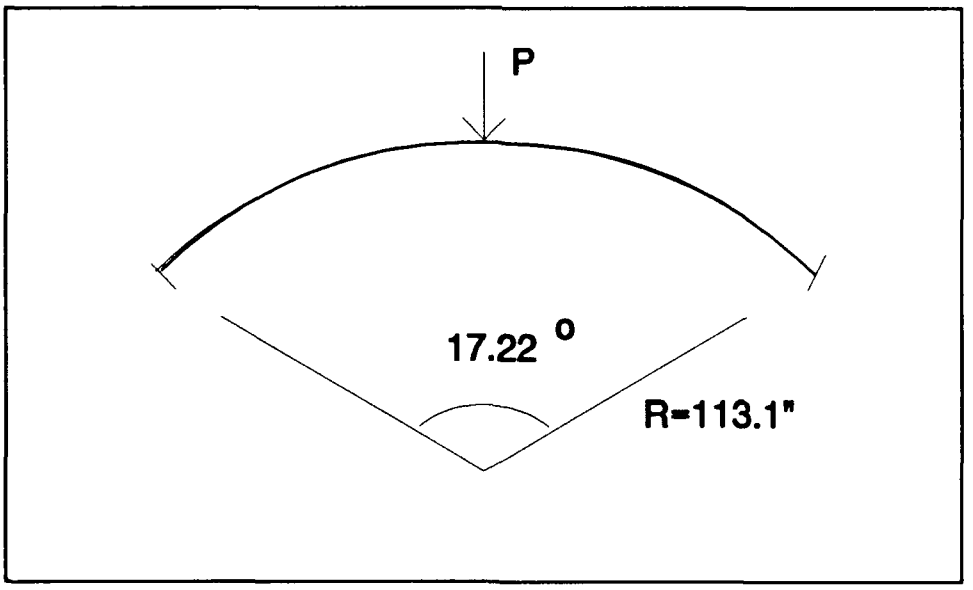

Figure 3-4. Clamped Isotropic Arch

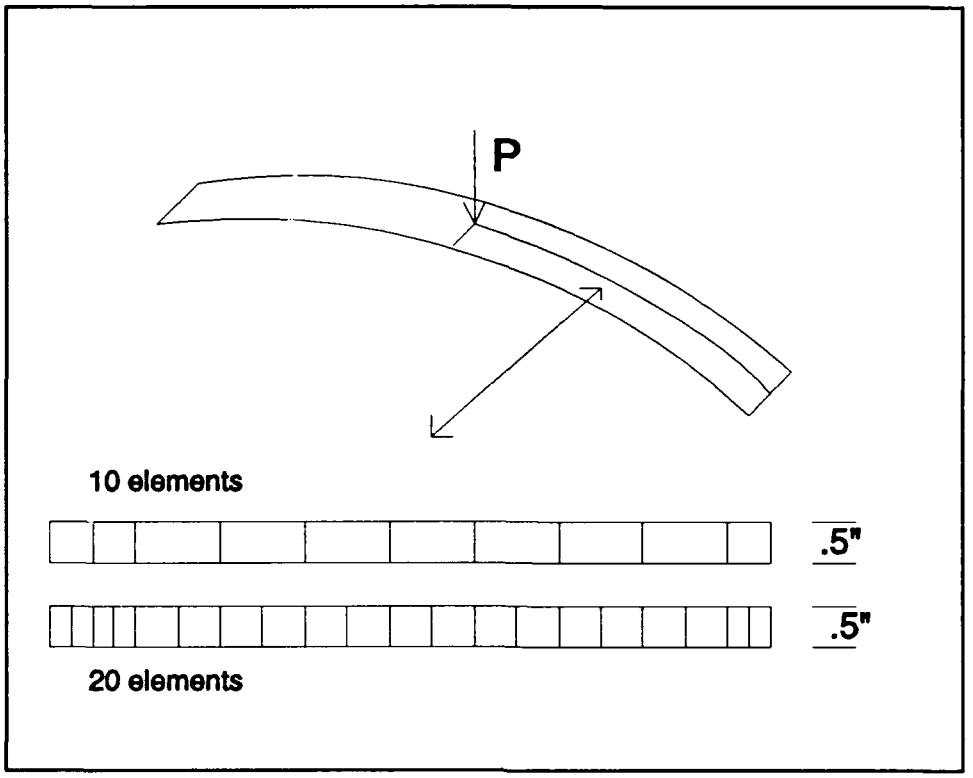

Figure 3-5. Mesh for Clamped Isotropic Arch

The loading is again applied radially inward at the center of the arch which results in the center of the arch displacing only radially. Fig (3-6) shows a comparison of the two load-displacement curves.

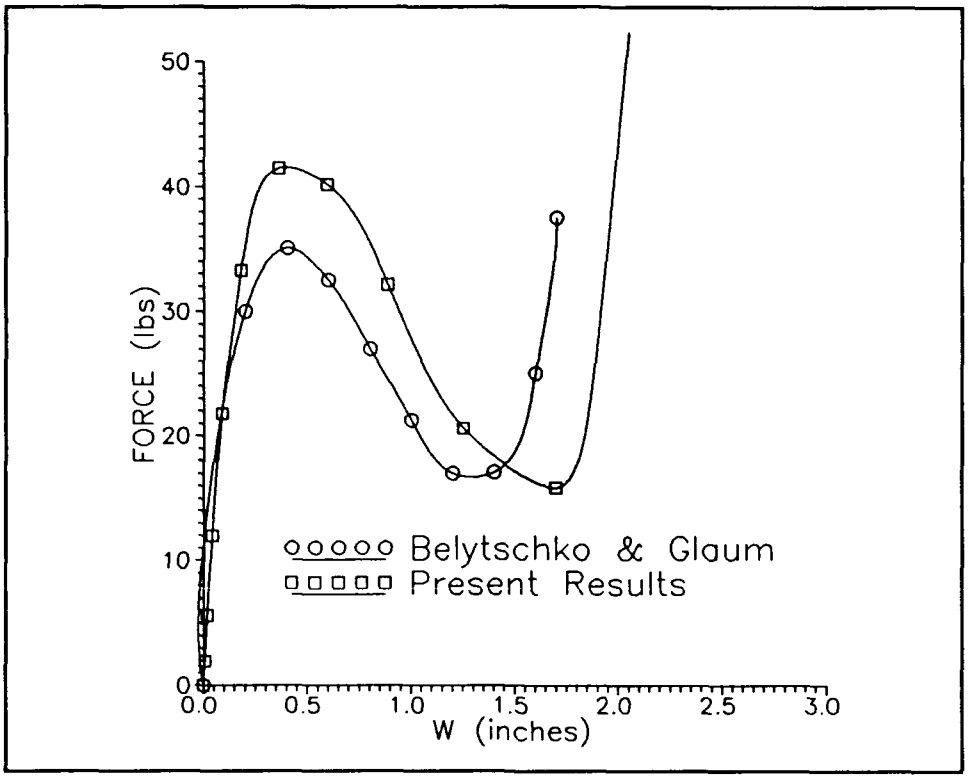

Figure 3-6. Load vs Displacement of Center Node, Clamped Isotropic Arch

As can be seen, the initial load-up for each formulation is approximately the same. The SHELL code calculates a higher buckling load because it includes nonlinear inplane displacement terms in the strain relations that are not included by Belytschko and Glaum which also does not include through the thickness shear terms. As the displacement becomes large a greater effect of extensibility in the SHELL element becomes present.

Dynamic Response of Isotropic Cylindrical Shell

A three inch thick isotropic cylindrical shell (shown in Fig 3-7) was subjected to a uniformly distributed half sine wave impulsive loading with peak intensity of 90 psf as shown in Fig (3-8).

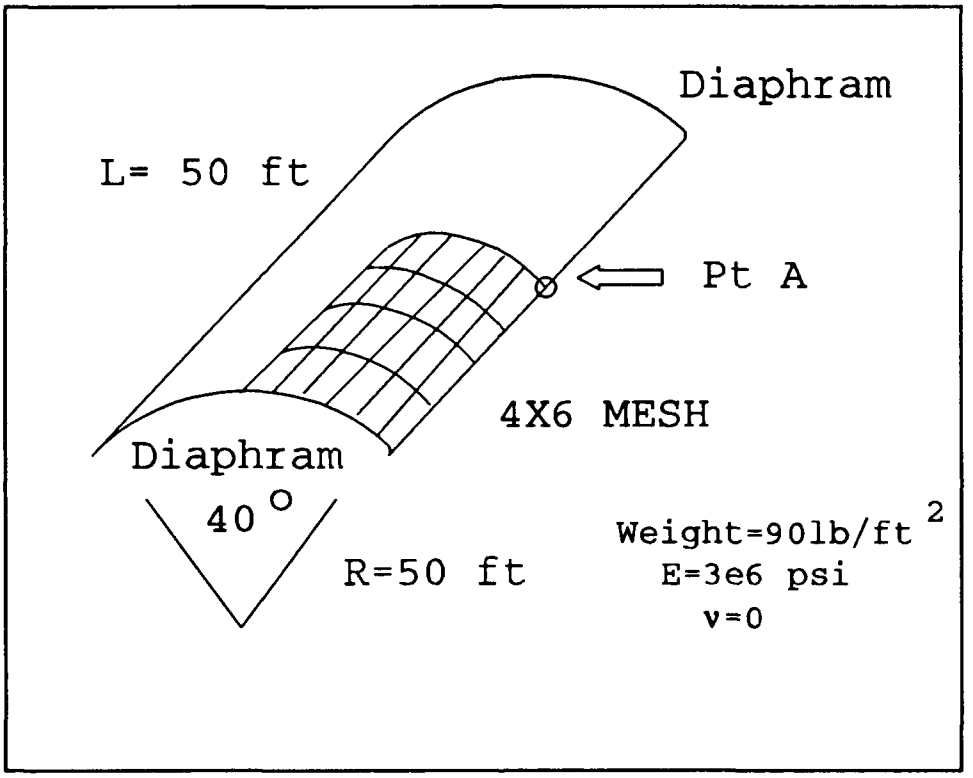

Figure 3-7. Isotropic Cylindrical Shell

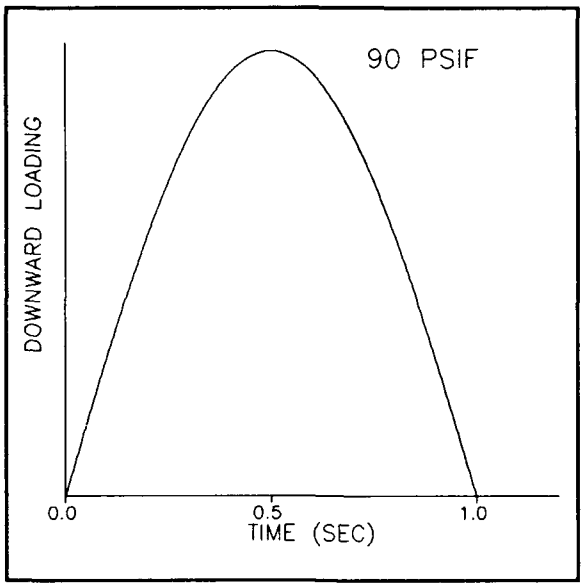

Figure 3-8. Loading for Isotropic Shell

Results are compared to existing results by Clough and Wilson (5), where through the thickness parabolic shear strain is not included. The two straight longitudinal edges were assumed free and the two circular edges were assumed to be supported on diaphragms. Material properties of E = 10.0E7 and ν = 0 are used. As done previously, 1/4 panel symmetry is taken advantage of. The time increment in each load step was 0.025 sec which is approximately 1/25 the first natural period of the shell.

The initial two analyses were accomplished without considering the inertia force, i.e. setting the mass terms to zero, thus they were effectively "static" analyses even

though the displacement changed with time. Both geometric linearity and non-linearity were considered by using SHELL's capability to either include or exclude the nonlinear terms in the strain-displacement relations. The results show good agreement and are presented in Fig (3-9).

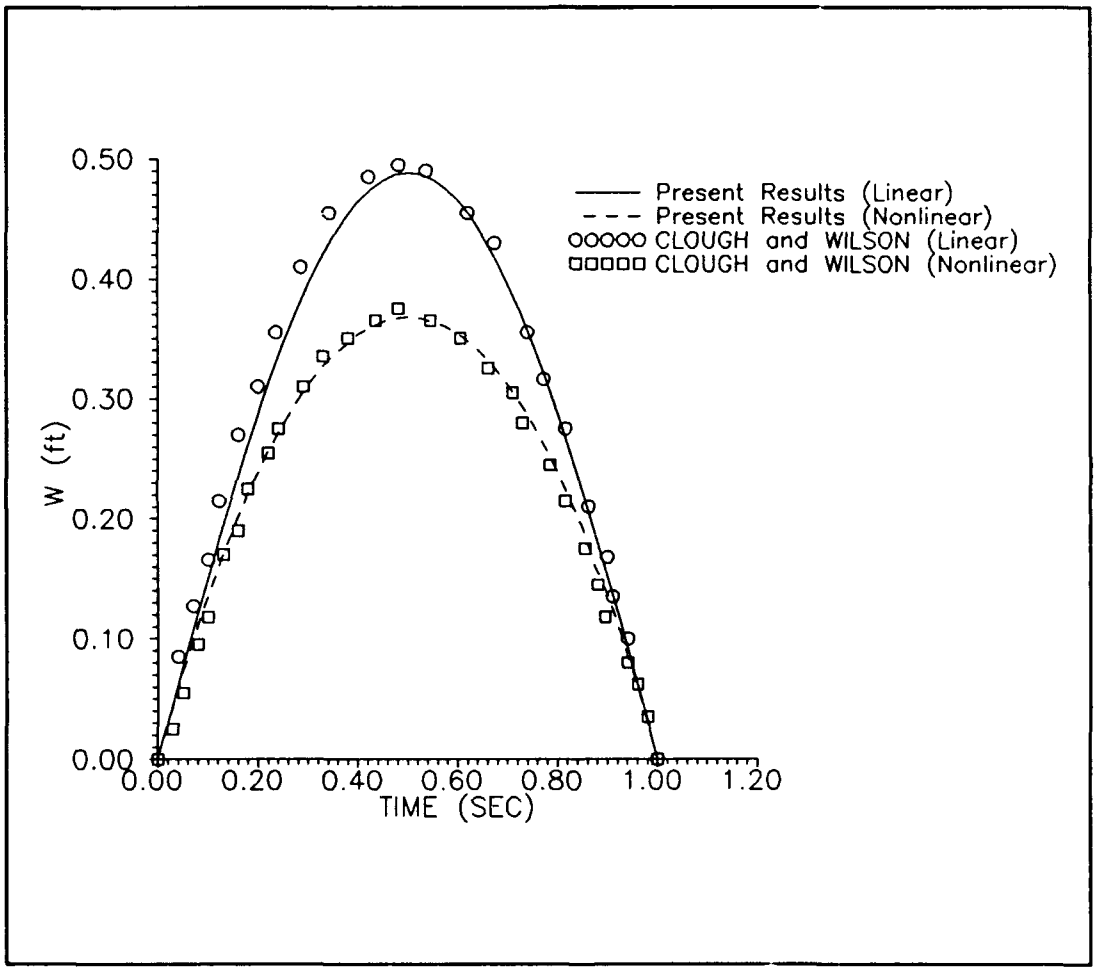

Figure 3-9. Displacement of Pt A vs Time, "Static"

Two additional analyses were carried out in which the mass density of the material is considered. The dynamic deflections are larger than static, as would be expected. Comparison with results from Clough and Wilson are shown in Fig (3-10). The agreement of results is due to the fact that transverse shear deformations are small for a shallow thin isotropic arch and the loading is well below the critical load which would cause snap-through.

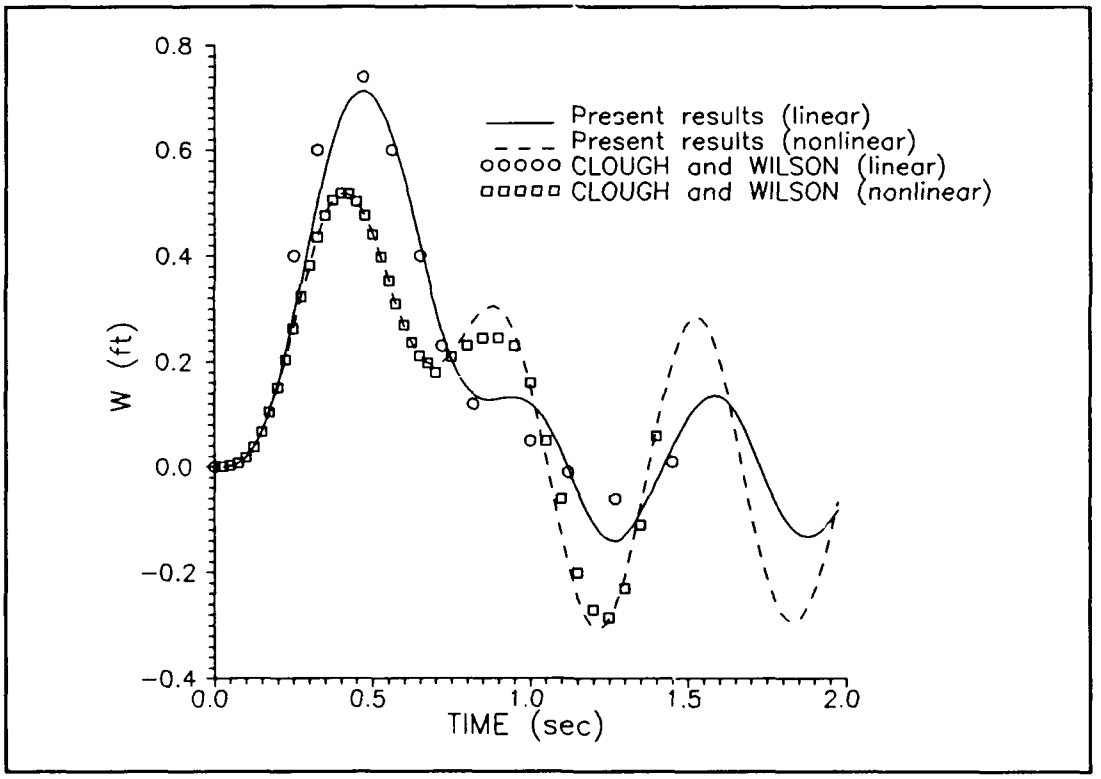

Figure 3-10. Displacement of Pt A vs Time, "Dynamic"

Critical Time Step

Before any further results are presented, it is important to discuss a parameter used in the numerical analysis of non-linear dynamics called the critical time step (Δt). Shell structures usually result in a so-called "stiff" system of differential equations where the highest eigenvalues determine the numerical stability of the explicit integration method (1). Therefore, a very small time step must be used. If the chosen Δt exceeds the critical value, a small error will be magnified with each time step and computed displacement will grow very rapidly and a numerical problem will be noticed after only a few time steps. If Δt is less than the critical value an error will not accumulate and the solution obtained will be reasonably accurate to the degree of tolerance used in the numerical scheme. Katona and Zienkiewkz (12) suggest using a Δt at most 1/12 times the first natural frequency of the structure. Reference (1) proposes several different methods for estimating the critical time step but concludes that once an initial estimate is made trial and error will most likely be necessary to further refine the critical time step. Dinkler and Kroplin (9) also point out that errors will grow uncontrollable unless a small time step is used but they also do not offer any explicit methods for determining Δt.

Laminated Arch

In this section, both the static and dynamic analysis of a simple supported laminated arch subjected to a center point load are presented.

Material. The analysis is performed on laminate constructed of high strength/low modulus Hercules AS4-3501-6 graphite epoxy with the following ply physical properties and dimensions:

ply thickness = 0.005 in.

E_1 = 18.844E6 psi

$E_2 = E_3$ = 1.468E6 psi

$G_{12} = G_{13}$ = 0.91E6 psi

G_{23} = 0.45E6 psi

ν_{12} = 0.28

$\nu_{21} = \nu_{31}$ = 0.0218

mass density = 0.00015088 slugs/in^3

Arch Geometry. A ply lay up of $[0_6/90_6]_s$ is used which has 24 plies and results in a total thickness of .12 inch. As shown in Fig (3-11) a radius of curvature of 12 in. along with an open angle θ of 1 radian is used. Width is the same order of thickness at .12 in. Mesh size for the quarter-arch ranged from 1" x .06" to .25" x .06" as shown in Fig (3-12).

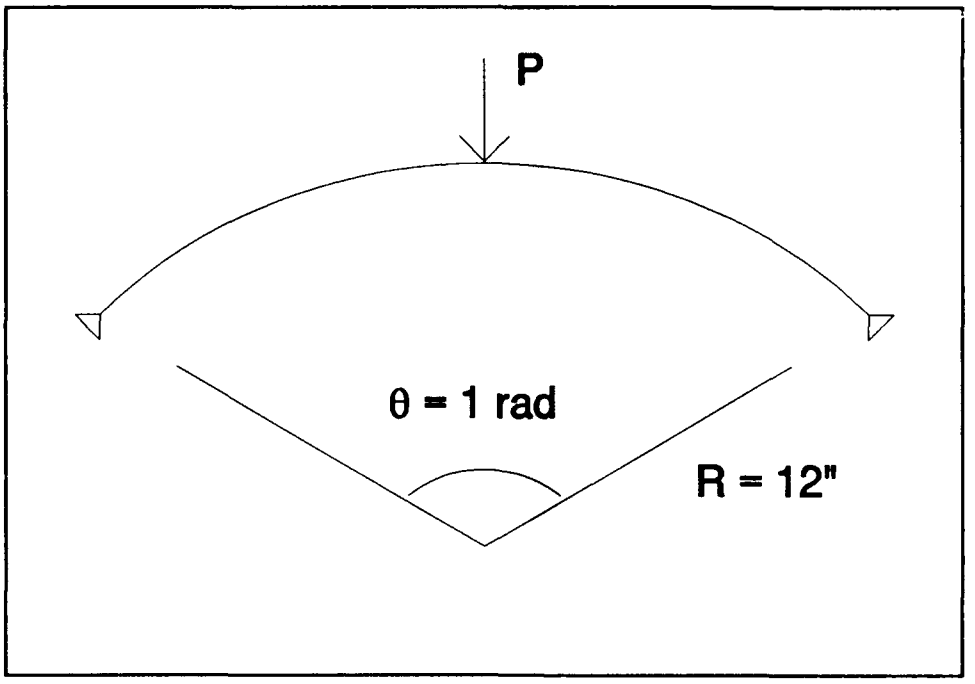

Figure 3-11. Laminated Arch

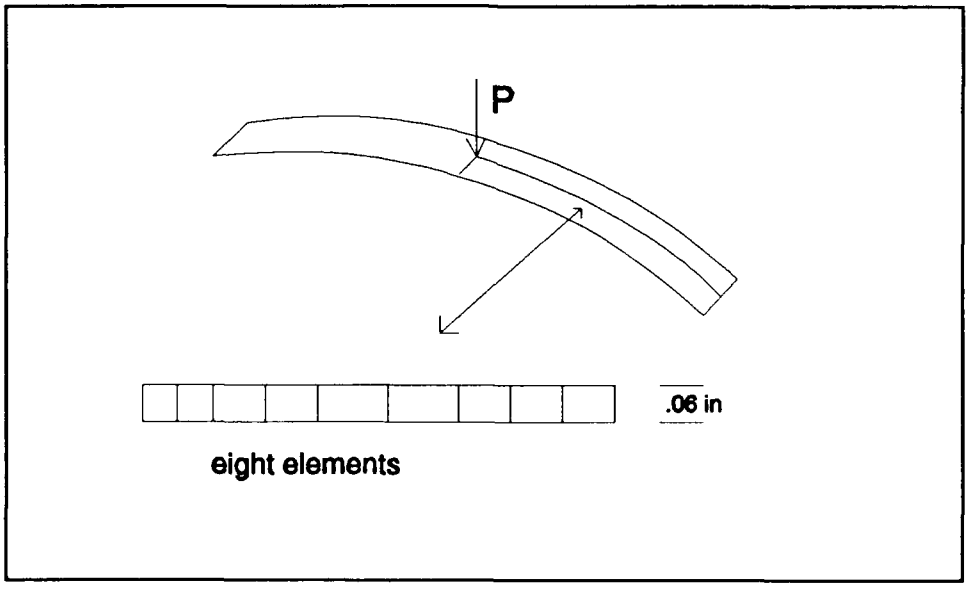

Figure 3-12. Mesh for Laminated Arch

Static Analysis. The SHELL code was used to investigate the static snap-through of the laminated arch. The static load-deflection curve is illustrated in Fig (3-13), which shows that the critical snapping load is approximately 11.5 lb.

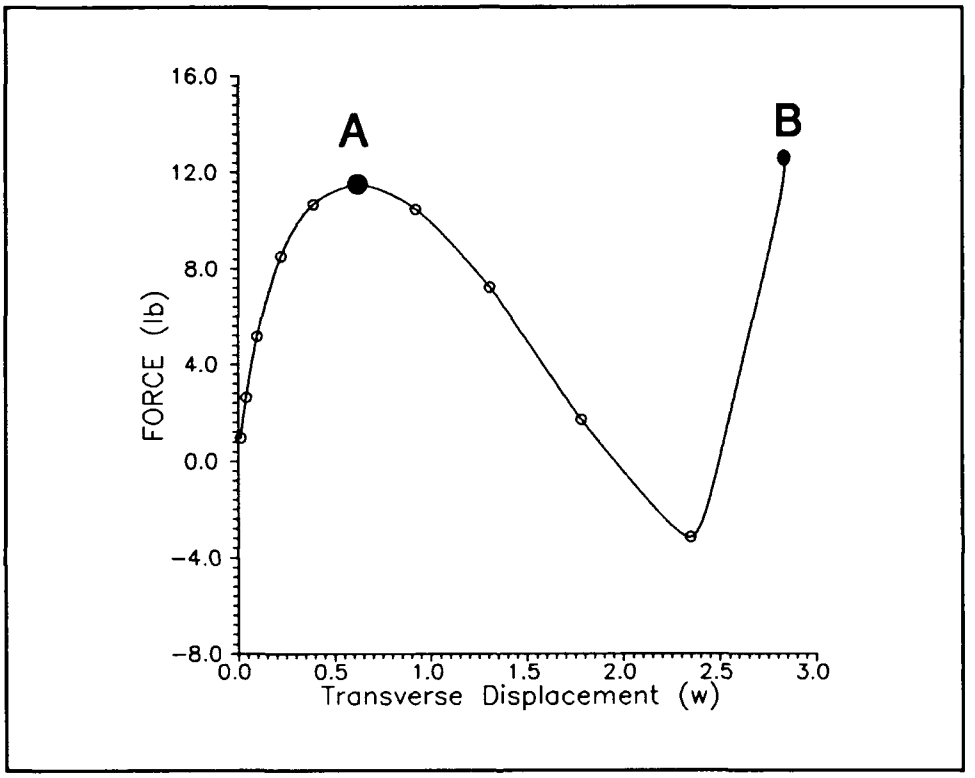

Figure 3-13. Load vs Displacement of Center Node, Laminated Arch

If a load slightly greater than 11.5 lb were applied it can be concluded from the curve that the shell should collapse and the center node should displace approximately 2.7 in. Figure 3-14 shows a profile of the centerline of

the arch at pt A and pt B from Fig (3-13) along with the original configuration.

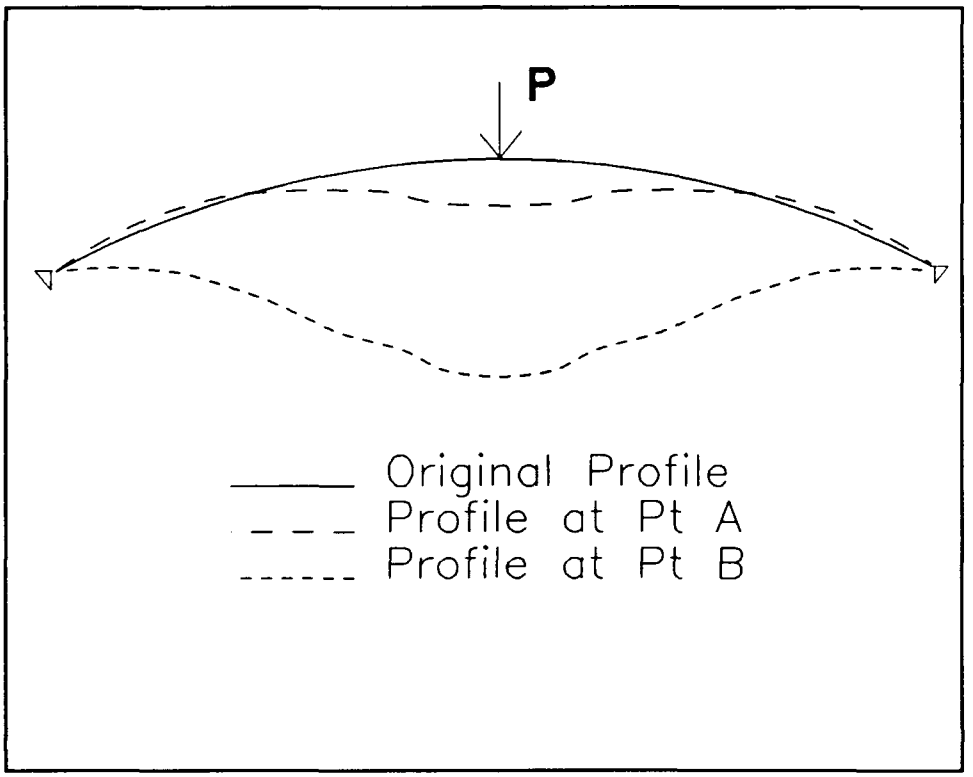

Figure 3-14. Centerline of Laminated Arch

The arch instantaneously snaps through from point A to B and is unstable until reaching point B where it is able to resume sustaining a load. As can be seen from Fig (3-14) the arch at point A is partly above and below its original configuration. This suggests that the part above is in compression and the part below is in tension. Once the arch has fully collapsed it is entirely in tension. Each point is below the original configuration.

Dynamic Analysis. The same problem subjected to dynamic loading is investigated. In the first case investigated, the applied dynamic loading history is shown in Fig (3-15), where the maximum load is smaller than the static critical snapping load.

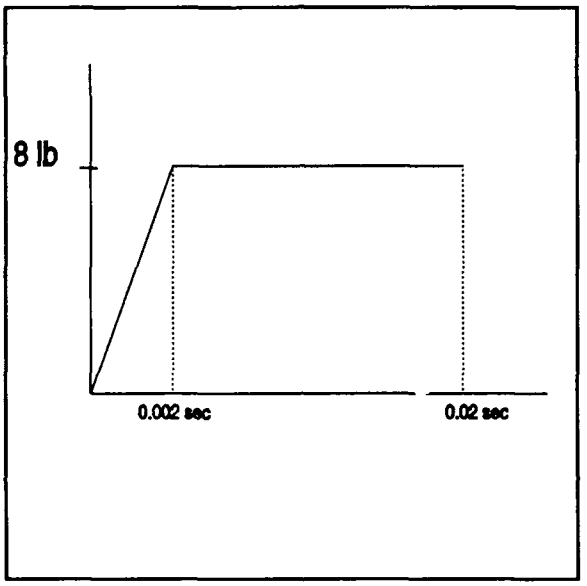

Figure 3-15. Loading History for Laminated Arch, Pre-buckling Load

The response is a regular smooth periodic vibration as shown in Fig (3-16). One curve shows a case where no damping is allowed and thus the amplitude of each period is the same and the other case shows that if damping is artificially imposed the steady state solution will result. A time increment of .0002 sec was used. Since the displacement

versus time curve displays good periodicity and the loading is less than critical where non-linear effects are not dominant, this time step was judged to be acceptable. As can be seen from the undamped case, approximately 17 points are plotted for each period which satisfies Katona and Zienkiewicz' (12) criteria of at least 12 per period. Thus,

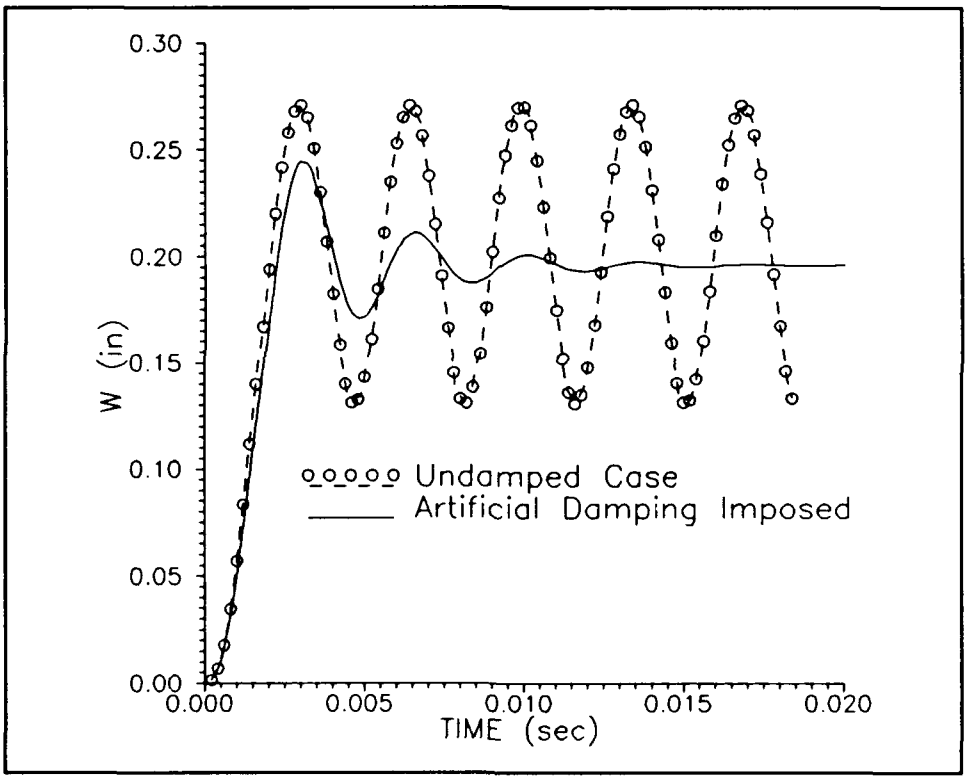

Figure 3-16. Displacement vs Time of Center Node for Laminated Arch, Pre-buckling Load

the natural frequency can be approximated at 294 Hz. An

eigenvalue analysis done by the SHELL code calculates the natural frequency at 499 Hz. Since the eigenvalue analysis uses only the linear terms in the stiffness matrix one would expect any calculations using the non-linear terms to predict a lower natural frequency.

In the second case analyzed, a maximum load of 12 lb is applied as shown in Fig (3-17), which is slightly greater than the critical snapping load of 11.5 lb.

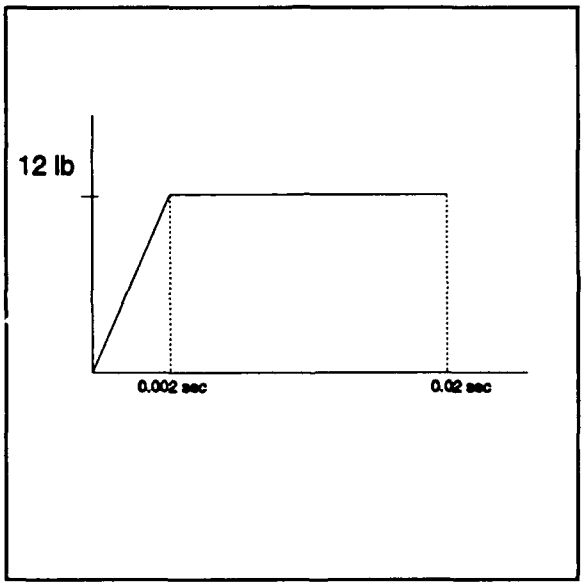

Figure 3-17. Loading History for Laminated Arch, Post-buckling Load

A time increment of 0.0002 sec is again used. During this phase of the research it was discovered that the percent convergence tolerance of the numerical technique is

very critical when investigating dynamic behavior due to loads above critical. Tolerances of 0.1 - 0.2 percent are acceptable when the load is sub-critical but this tolerance range causes errors to grow uncontrollable when the load is above critical. It becomes obvious that the solution "breaks down" before representing a realistic dynamic pattern. Fig (3-18) shows a comparison of the time versus center node displacement history obtained using a percent convergence tolerance of 0.1 and 0.0001. The 0.1 percent curve "breaks down" shortly after reaching the peak displacement. As can be seen error grows uncontrollably and the curve no longer represents a realistic solution. The 0.0001 percent curve calculates two realistic vibration periods before it was no longer able to converge to the desired tolerance.

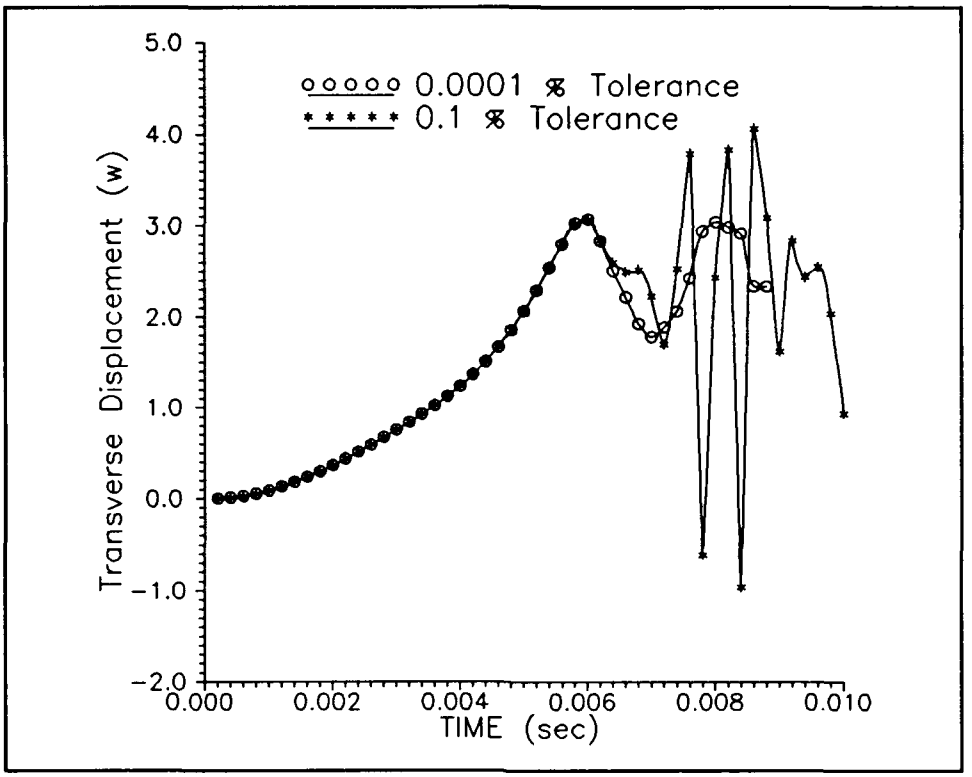

Figure 3-18. Center Node Displacement vs Time, Laminated Arch

Fig (3-19) shows the time vs displacement history for both an undamped and artificially damped case using the percent convergence tolerance of 0.0001. The damping coefficient imposed is 0.1. Because the non-linear parts of the strain-displacement relations are dominant and the solution technique is numerical, a pure sinusoidal curve is not seen but it is approximated. The reason as to why the two cases do not average the same displacement is as yet unresolved. As can also be seen, the initial curve leading up to the maximum displacement is concave up. This

demonstrates that the nonlinear kinematics are producing a more flexible arch response relative to linear relations.

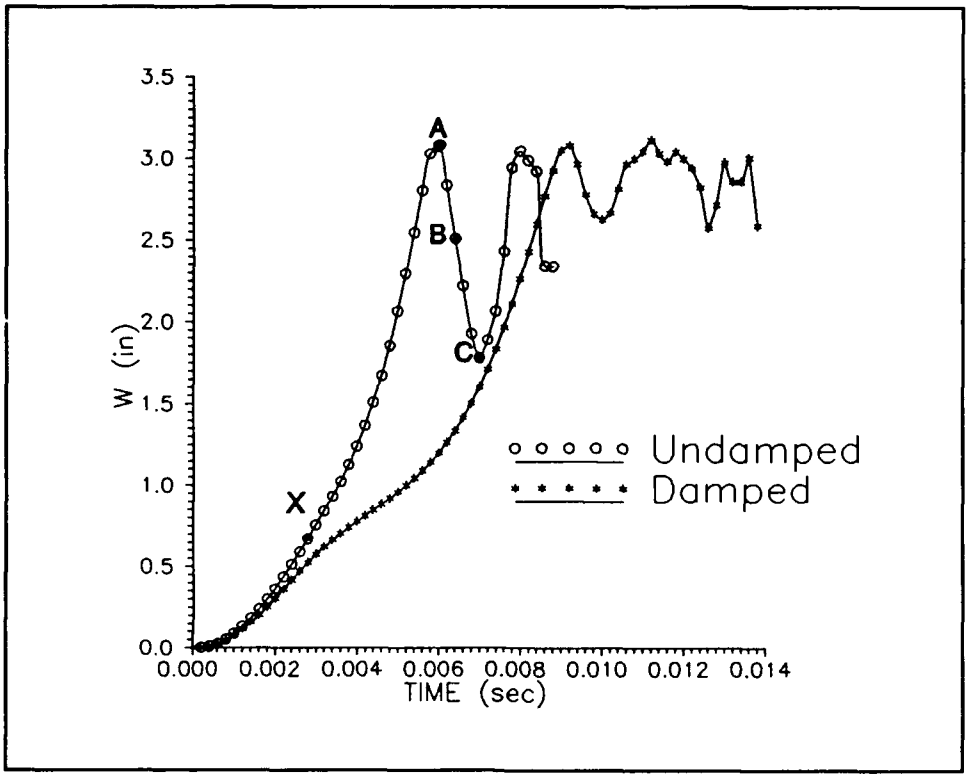

Figure 3-19. Displacement vs Time of Center Node, Laminated Arch, Post-buckling Load

Fig (3-20) shows a profile of the arch centerline at points A, B, and C from Fig (3-19). As can be seen, the centerline at point B, which is at approximately the average amplitude, closely resembles that from Fig (3-14). However, it is unclear why the displacement at point B, which is at the average amplitude for the undamped case, is 2.5 inches while the static curve suggests a collapse displacement of 2.7 inches.

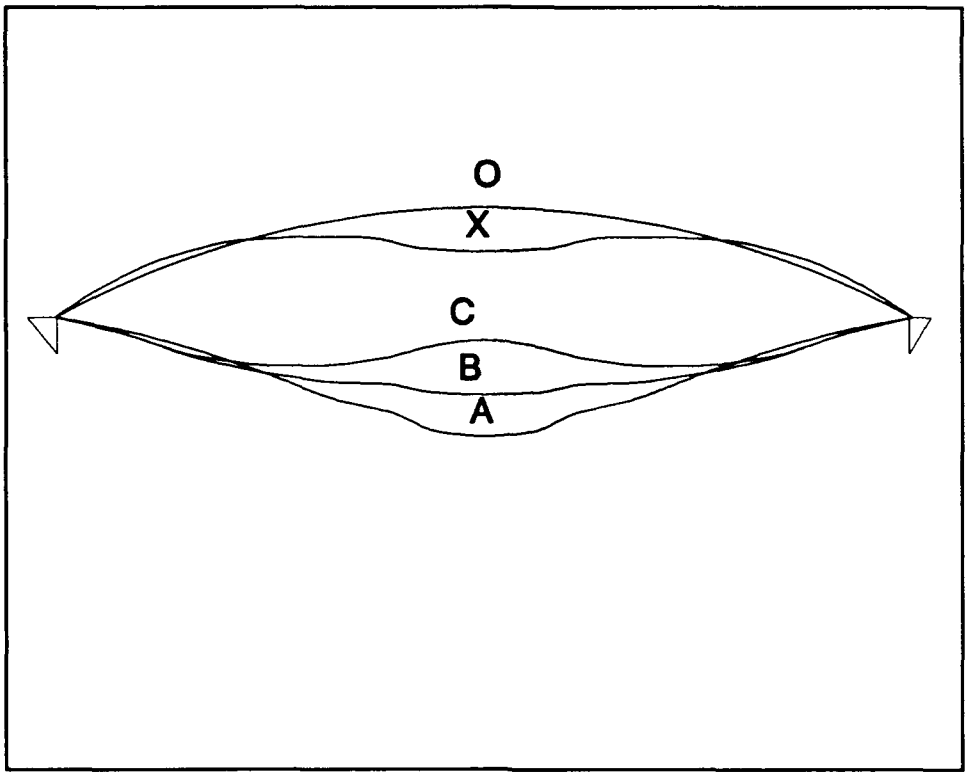

Figure 3-20. Profile of Laminated Arch Centerline

Fig (3-20) also shows that only the middle third of the arch appears to be in vibration. There are two counter flecture points approximately 1/3 in from each boundary where the bending moment remains near zero. Also shown is a profile of the arch corresponding to point X on Fig (3-19) which is immediately after the onset of the maximum load. This profile closely resembles the pre-buckling profile from Fig (3-14). This profile does not appear immediately after the onset of the critical load because the dynamic calculations take into account inertia forces but it does indicate the start of the snapping phenomena.

Laminated Cylindrical Shell

The final case investigated is that of a laminated cylindrical shell subject to a center point load. The material studied is the same as the laminated arch and presented again below:

ply thickness = 0.005 in.

$E_1 = 18.844 \times 10^6$ psi

$E_2 = E_3 = 1.468 \times 10^6$ psi

$G_{12} = G_{13} = 0.91 \times 10^6$ psi

$G_{23} = 0.45 \times 10^6$ psi

$\nu_{12} = 0.26$

$\nu_{21} = \nu_{31} = 0.0218$

mass density = 0.00015088 slug/in^3

Geometry and Boundary Conditions. The same ply lay-up as the arch was used of $[0_6/90_6]_s$ resulting in an overall shell thickness of 0.12 in. Again a radius of curvature of 12 inches is used along with an open angle θ of 1 radian as shown in Fig (3-21). A length of 18 inches is used so results can be compared to Silva (23) who ran the same static analysis on the SHELL code. Both straight edges were allowed to be simply supported while both curved edges were allowed to be free. This combination of geometry, ply-layup, and boundary conditions were chosen because it was shown by Silva to fully collapse. "Full" collapse is said

to occur when the free ends also turn under which implies that every point in the shell has displaced below its original configuration.

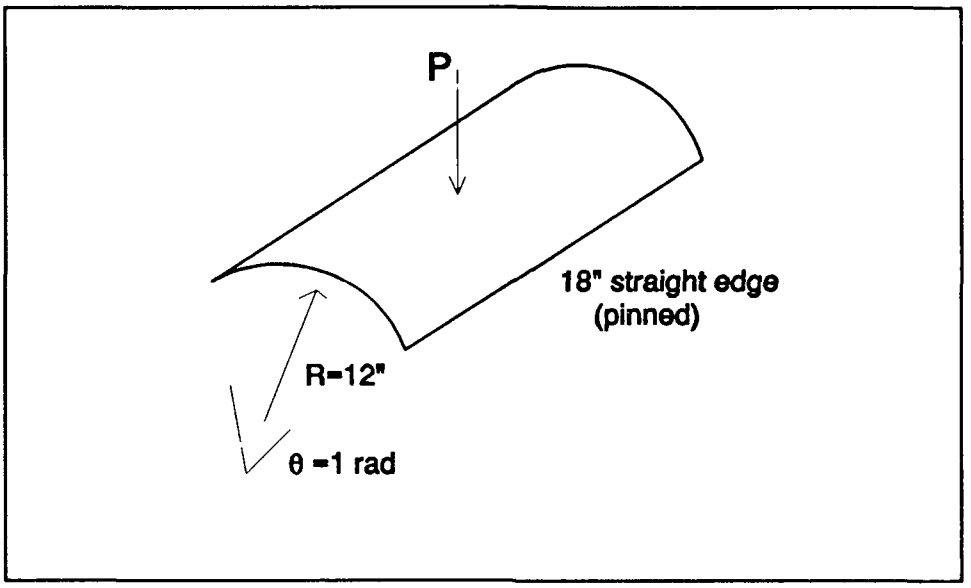

Figure 3-21. Laminated Shell Geometry

Finite Element Mesh. As seen in Fig (3-21), Silva uses an 88 element 1/4 panel mesh to achieve a static load versus displacement curve. In an effort to reduce the necessary computer run time, particularly for the dynamic analysis, the present work reduces the number of elements to a 49 element mesh. Although the number of degrees of freedom in this mesh does not fall within the convergence criteria set by Silva (23), it does fall within 5 percent of his criteria based on peak load. Silva uses elements ranging in size

from 1"x1" to ½"x½" while the present work uses elements that range in size from 2"x1" to ½"x½". It should be noted that in the area of point load application the element size for both meshes is ½"x½".

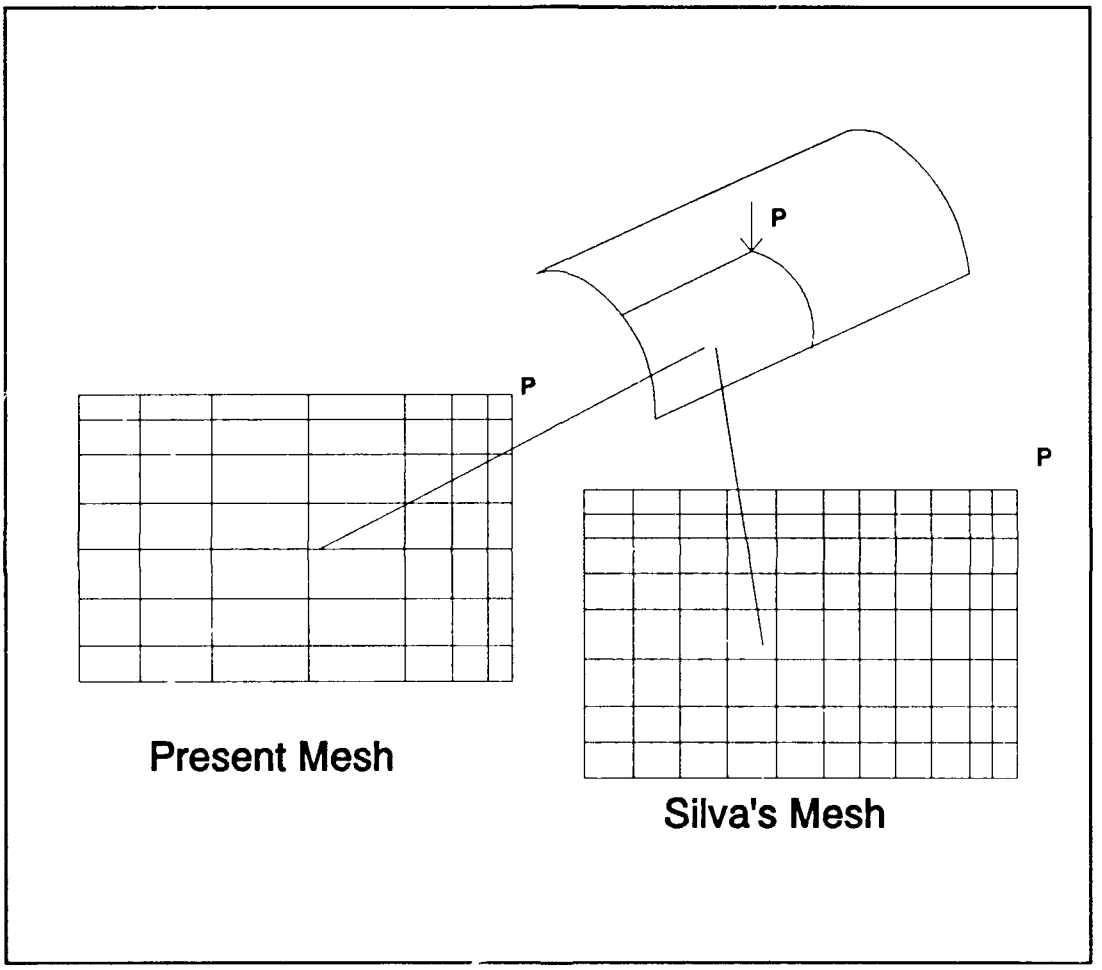

Figure 3-22. Mesh Comparison for Laminated Shell

Static Analysis. Fig (3-23) shows the static load versus displacement curves for both Silva's analysis and the present work. The initial load up and critical load are approximately the same but with less finite elements the post buckling behavior is slightly more difficult to track. The critical snapping load is calculated to be approximately 2800 lb. The initial post buckling deflection of the center node is approximately 2.7 in.

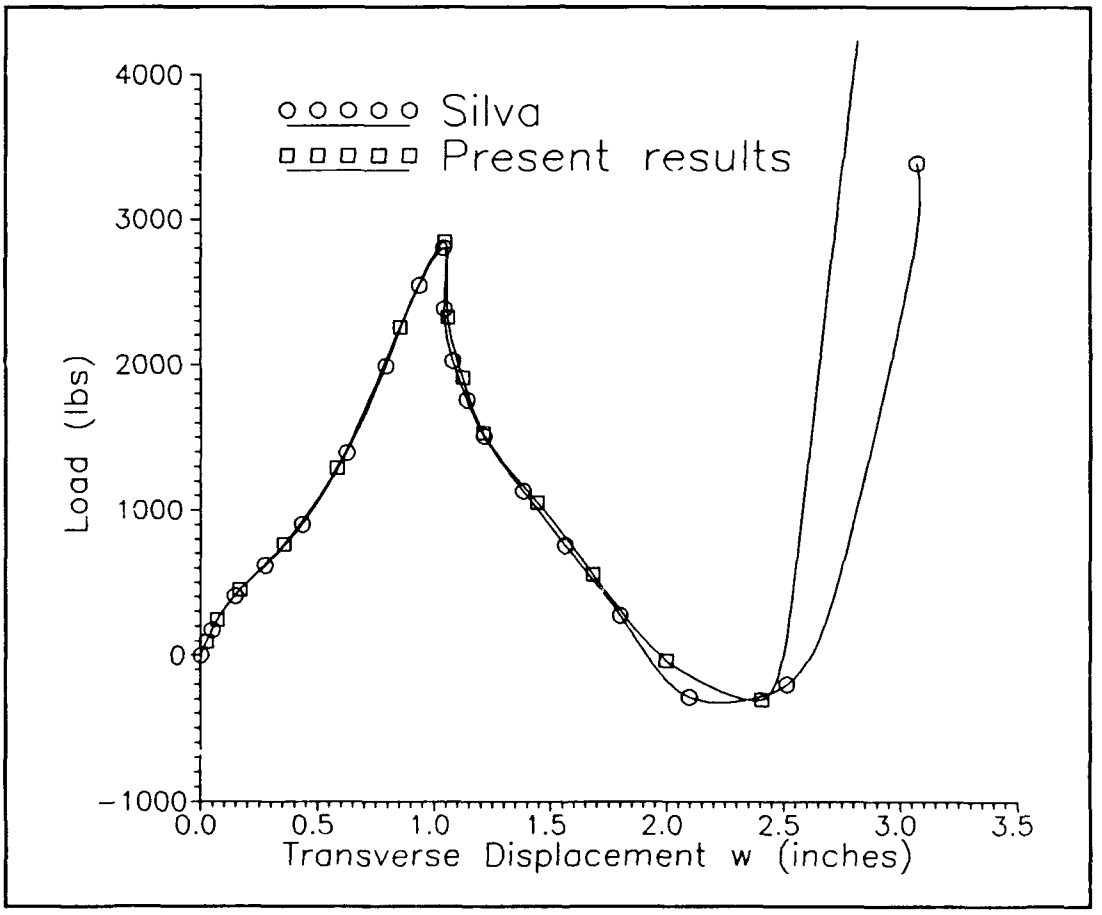

Figure 3-23. Load vs Displacement, Cylindrical Shell

Dynamic Analysis. The same problem subjected to dynamic loading is investigated. For the first analysis, the applied dynamic loading history, shown in Fig (3-23), is smaller than the static critical snapping load. The response, as shown in Fig (3-24), is periodic, but not

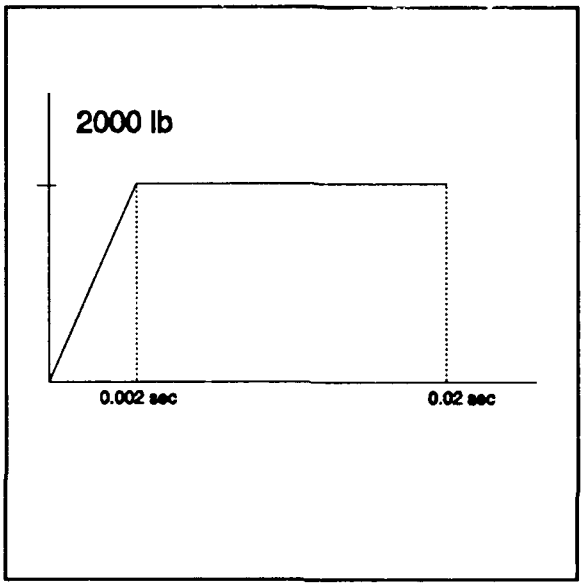

Figure 3-24. Loading History for Cylindrical Shell, Pre-critical Load

purely sinusoidal. The fact that the curve is not purely sinusoidal can perhaps be accounted for due to the large number of calculations performed, the non-linearity of the strain-displacement equations, the precision of the computer code (double precision is used) and the round-off error of the computer. The average displacement for each period does

however, match that for the static load vs deflection curve of Fig (3-23) which indicates that steady state has been reached.

A time step of 0.0002 seconds is presented however the results were the same when a time step of 0.0001 sec was used thus convergence is assumed. By approximating the time between peaks, a natural frequency of 225 Hz is estimated. Again an eigen value analysis predicts a higher natural frequency of 505 Hz.

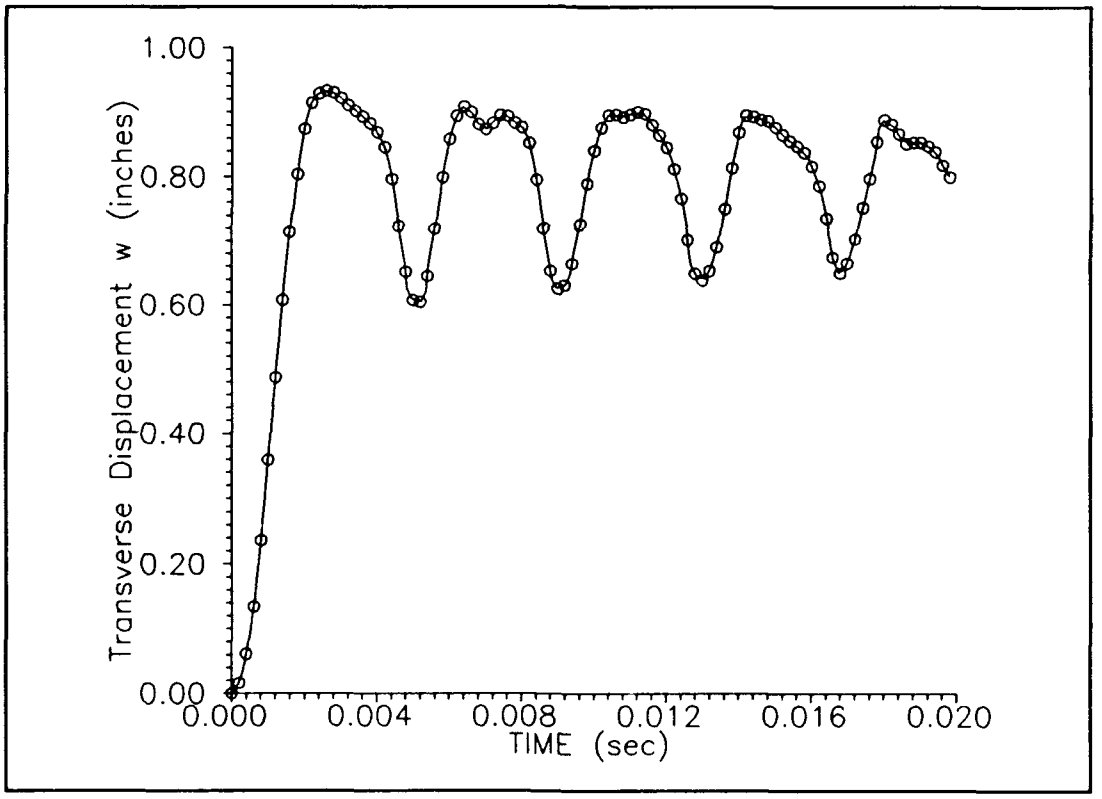

Figure 3-25. Displacement vs Time of Center Node, Cylindrical Shell, Pre-critical Loading

In the second analysis, the applied dynamic loading history is greater than the static critical snapping load as shown in Fig (3-26). Time steps of 0.0002 sec and 0.0001 sec were used. A percent tolerance of 0.001 was imposed.

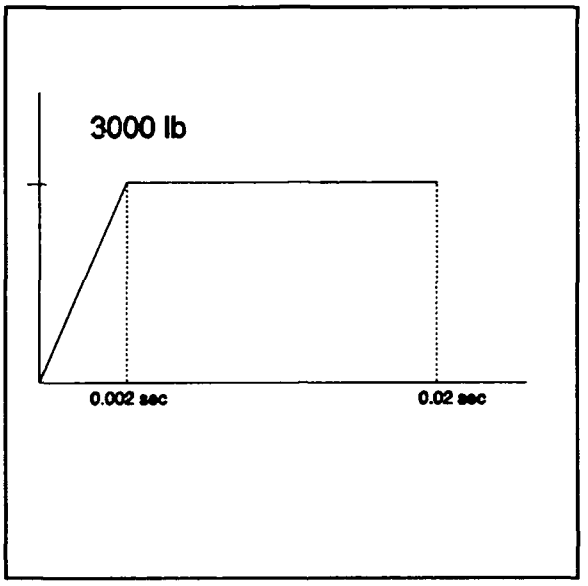

Figure 3-26. Load History for Cylindrical Shell, Post-Buckling Load

The vibration response of the shell is shown in Fig (3-27). The curve representing the time step of 0.0002 sec "breaks down" after reaching the maximum displacement and is not able to show any reasonable periodicity. By cutting the time step in half to 0.0001 seconds the curve is able to show approximately one and one-half cycles before it also reaches a point where the error goes uncontrollable.

However, during the one and one-half periods the average amplitude of 2.7 inches matches that of the static load displacement curve of Fig (3-23).

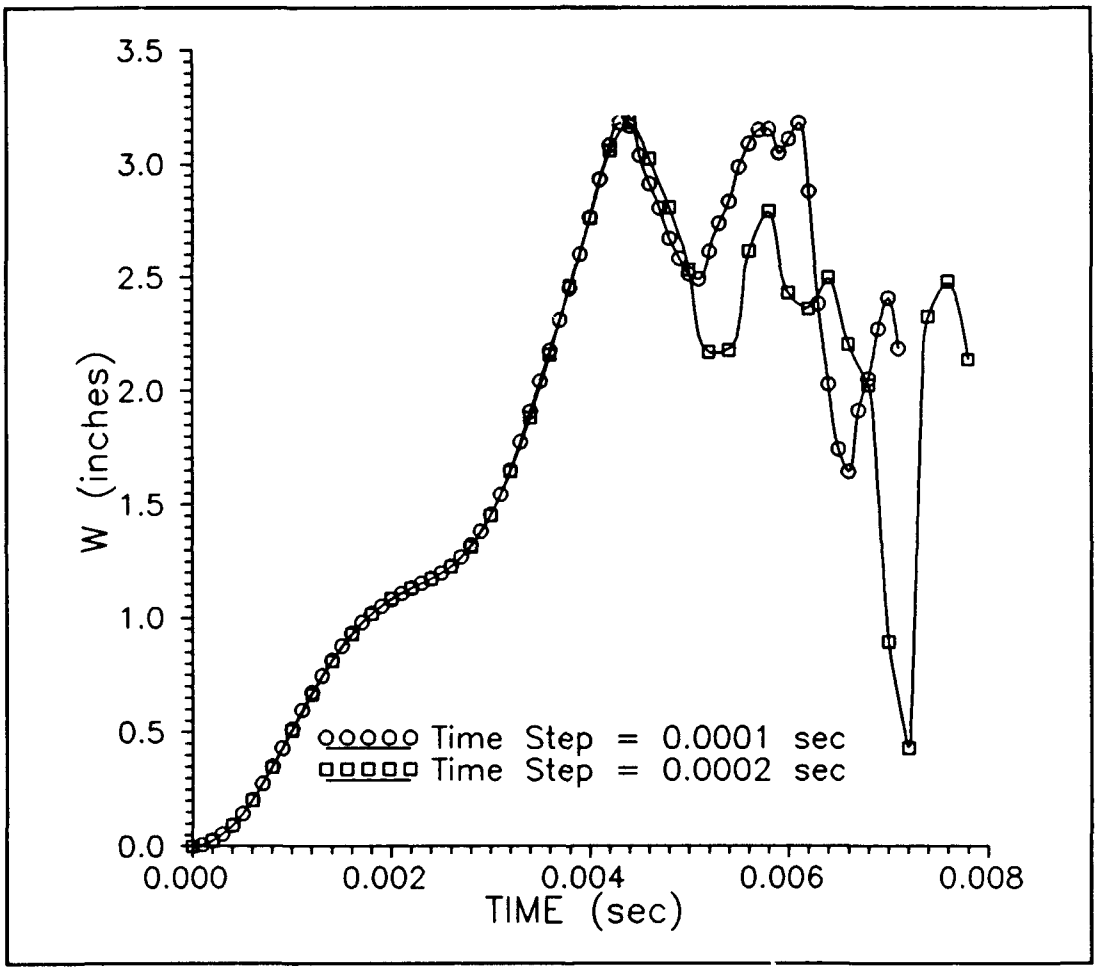

Figure 3-27. Displacement vs Time of Center Node, Cylindrical Shell, Post-buckling Load

At this point it is as yet unresolved as to whether

decreasing the time step even further would yield even more realistic results or the limits of the numerical precision of the computer have been reached.

IV. CONCLUSIONS/RECOMMENDATIONS

Conclusions

The instability of thin laminated cylindrical shells acted upon by transverse loads is clearly a dynamic phenomena for which analytical prediction and physical reality have yet to be fully reconciled. Some authors prefer to investigate the post buckling state using a static analysis while others argue that only a dynamic analysis is able to cope with the difficult phenomena of transient multimode buckling between the pre- and post-buckling range. It is apparent that this argument becomes very significant when instability of a shell is considered with transverse loading. It is also a major characteristic when one investigates cylindrical panels acting under axial compression. With the SHELL code, it is possible to use the same set of constitutive laws, strain-displacement relations, and finite element formulations to do both a static and dynamic analysis on a particular shell. The resulting comparison gives insight into the post buckling behavior of shells and their ability to sustain a load after collapse. An exclusively static analysis is a useful tool for predicting the immediate post buckling state in a dead load situation. However, such an analysis considers only static equilibrium states. Beyond the critical load point

it is concerned with equilibrium states which may or may not occur as the shell dynamically seeks another configuration in which it can resume supporting a load. On the other hand, a dynamic analysis is not concerned with these artificial equilibrium states and can trace the behavior of the shell all the way through the buckling process. It should be noted though, that the dynamic analysis requires significantly more computer time than a static analysis. In a numerical scheme, the time step must be small enough to avoid numerical instability. It has been shown that in using the SHELL code, the response of a shell resulting from a dynamic steady state analysis subjected to a step load, matches the displacement on the snap through load versus displacement curve.

Recommendations

There are many parameters involving the use of the SHELL dynamic code which lend themselves as areas of further study. The effect of boundary conditions, other than simply supported, require further study. For example, a shell that is clamped on the edges will respond differently and is perhaps more common in aircraft structures. Also, various load conditions such as line and distributed loads should be investigated. An impulse load can also be used other then a step load. The use of a damping factor requires further study particularly in trying to get a physical meaning of

the phenomena. Perhaps the most important area requiring further study is that of the numerical integration scheme and its inherent numerical instability. More investigation into the tolerance and the critical time step are needed. Also, the use of different parameters for the beta-m integration technique might cause convergence to a solution at a faster rate.

Bibliography

1. Almroth, B.L., F.A. Brogan, and G.M. Stanley, User Instructions for STAGSC-1, Volume II, LMSC-DG33873, pp 6-32 - 6-37, January, 1983.

2. Bathe, K.J. and L.W. Ho. "Some Results in the Analysis of Thin Shell Structures," Nonlinear Finite Element Analysis in Structural Mechanics, ed. W. Wunderlich, E. Stein, and K. J. Bath, 1981, Springer-Verlag Berlin, Heidelberg, NY, pp. 122-150.

3. Belytschko, T. and L.W. Gluam,"Applications of Higher Order Corotational Stretch Theories to Nonlinear Finite Element Analysis," Computers and Structures, Vol 10, 175-182, 1979.

4. Chung, S. and O. Widera. "A Theory for Non-Homogeneous Anisotropic Cylindrical Shells," Journal of Composite Materials, Vol 6, 14-30, 1963.

5. Clough, R.W. and E.L. Wilson. "Dynamic Finite Element Analysis of Arbitrary Thin Shells, " Computers and Structures, Vol 1, 33-56, 1971.

6. Cook, R.D., D.S. Malkus, and M.E. Plesha. Concepts and Applications of Finite Element Analysis, John Wiley and Sons, 1989.

7. Crisfield, M.A. "A Fast Incremental/Iterative Procedure That Handles 'Snap-Through'," Computers and Structures, Vol 13, 55-62, 1981.

8. Dennis, S.T. Large Displacement and Rotational Formulation for Laminated Cylindrical Shells Including Parabolic Transverse Shear, D.S. Thesis AFIT/DS/AA/88-1. School of Engineering, Air Force Institute of Technology (AU), Wright Patterson AFB, OH, 1988.

9. Dinkler, D. and B. Kroplin. "Dynamic Versus Static Buckling Analysis of Thin Walled Shell Structures," Finite Element Methods for Plate and Shell Structures, Volume 2: Formulations and Algorithms, ed. E. Hinton and T.J.R. Hughes, Pineridge Press International, 1986, pp. 229-251.

10. Donnell, L.H. Stability of Thin-Walled Tubes Under Torsion. NACA Report 479, 1933.

11. Kapania, R.K., and Raciti, S. "Recent Advances in Analysis of Laminated Beams and Plates, Part I: Shear Effects and Buckling," AIAA Journal, Vol 27, No 7, July 1989.

12. Katona, M.G., and Zienkiewicz, O.C. "A Unified Set of Single Step Algorithms, Part 3: The Beta-m Method, a Generalization of the Newmark Scheme," International Journal for Numerical Methods in Engineering, Vol. 21, 1345-1359, 1985.

13. Nayfeh, A.H., and D.T.Mook Nonlinear Oscillations, Wiley, 1979

14. Tsai, C.T. and Palazotto, A.N. "On the Finite Element Analysis of Nonlinear Vibration for Cylindrical Shells with High-order Shear Deformation Theory," accepted for publication in International Journal of Nonlinear Mechanics.

15. Ramm, E. "Strategies for Tracing the Nonlinear Response Near Limit Points," Nonlinear Finite Element Analysis in Structural Mechanics, ed. W. Wunderlich, E. Stein, and K.J. Bathe, 1981, Springer - Verlag Berlin, Heidelberg, NY, pp. 63-89.

16. Reddy, J.N. Energy and Variational Methods in Applied Mechanics with an Introduction to the Finite Element Method, Wiley, 1984.

17. Reddy, J.N. and C.F. Liu. "A Higher Order Shear Deformation Theory of Laminated Composite Shells," International Journal of Engineering Science, Vol 23, No 3, 319-330, 1985.

18. Riks, E. "The Application of Newton's Method to Nonlinear Theories of Solids," Journal of Applied Mechanics Vol 39, 1060-1065, 1972.

19. Riks, E. "An Incremental Approach to the Solution of Snapping and Buckling Problems," International Journal of Solids and Structures, Vol 15, 529-551, 1979.

20. Saada, A.S. Elasticity Theory and Applications, Pergamon Press, 1974.

21. Sabir, A.B. and A.C. Lock. "The Application of Finite Elements to the Large Deflection Geometrically Non-linear Behavior of Cylindrical Shells," Variational Methods in Engineering, ed. C. Brebbia and H. Tottenham, Southampton University Press, 1973, pp. 7/66-7/75.

22. Sanders,J.L. An Improved First Approximation Theory for Thin Shells. NASA TR-24, 1959.

23. Silva, K.J. Finite Element Investigation of a Composite Cylindrical Shell Under Transverse Load with Through Thickness Shear and Snapping. MS Thesis, AFIT/GAE/ENY/89D-35. School of Engineering, Air Force Institute of Technology (AU), Wright Patterson AFB, OH, 1989.

24. Simmons, J.G. "A Set of Simple, Accurate Equations for Circular Cylindrical Shells," International Journal Of Solids and Structures, Vol. 2, 522-541 (1966)

25. Schimmels, S.A. Investigation of Collapse Characteristics of Cylindrical Composite Panels with Large Cutouts. MS Thesis, AFIT/GAE/ENY/89D-33. School of Engineering, Air Force Institute of Technology (AU), Wright Patterson AFB, OH, 1989

26. Tsai, C.T. and A.N. Palazotto. "A Modified Riks Approach to Composite Shell Snapping Using Higher Order Shear Deformation Theory," Computers and Structures, Vol 35, No 3, 221-226, 1990.

27. Wempner, G.A. "Discreet Approximations Related to Nonlinear Theories of Solids," International Journal of Solids and Structures, Vol 7, 1581-1599, 1971.

Vita

Major Walter W. Taylor Jr. [redacted] He graduated from high school in Braintree, Massachusetts, in 1975 and accepted an appointment to the United States Air Force Academy in Colorado. After earning his Bachelor of Science Degree in Engineering Mechanics in May 1979 he served the Air Force as an aeronautical engineer at the Air Force Weapons Laboratory, Kirtland AFB, New Mexico. After graduating from USAF pilot training at Reese AFB, Texas in August 1983 Major Taylor served as a C-141B pilot at McGuire AFB, New Jersey. Major Taylor entered the Air Force Institute of Technology, School of Engineering in May 1989.

[redacted]

December 1990 Master's Thesis

FINITE ELEMENT INVESTIGATION INTO THE DYNAMIC INSTABILITY CHARACTERISTICS OF LAMINATED COMPOSITE PANELS

Walter W. Taylor Jr., Major, USAF

Air Force Institute of Technology
WPAFB OH 45433-6583

AFIT/GAE/ENY/90D-28

Spencer T. Wu
AFOSR/NA
Bolling AFB, Washington DC 20332-6448

Dynamic instability of a laminated composite panel subjected to a transverse load is studied. Up to cubic variations in the thickness coordinate are included in the inplane displacement field, and only the constant component is kept in the transverse displacement. The transverse shear strains retain only linear displacement terms and vary parabolically through the thickness. The complete quadratic displacement functions are included in the inplane strains. A 36 degree of freedom shell element is used to obtain numerical results. The static snap through load vs displacement curve, as well as the critical collapse load, is examined by invoking the Riks technique along with the Newton-Raphson iteration scheme. The beta-m time marching integration method is employed to evaluate a dynamic response. Two step loads, with the step magnitude slightly below and above the critical collapse load, are introduced in the dynamic analysis. The response resulting from the dynamic analysis matches the displacement on the static load vs displacement curve.

Nonlinear Analysis, Vibration, Finite Element Analysis, Shells, Structural Mechanics 94

Unclassified Unclassified Unclassified UL

GENERAL INSTRUCTIONS FOR COMPLETING SF 298

The Report Documentation Page (RDP) is used in announcing and cataloging reports. It is important that this information be consistent with the rest of the report, particularly the cover and title page. Instructions for filling in each block of the form follow. It is important to **stay within the lines to meet optical scanning requirements.**

Block 1. Agency Use Only (Leave Blank)

Block 2. Report Date. Full publication date including day, month, and year, if available (e.g. 1 Jan 88). Must cite at least the year.

Block 3. Type of Report and Dates Covered. State whether report is interim, final, etc. If applicable, enter inclusive report dates (e.g. 10 Jun 87 - 30 Jun 88).

Block 4. Title and Subtitle. A title is taken from the part of the report that provides the most meaningful and complete information. When a report is prepared in more than one volume, repeat the primary title, add volume number, and include subtitle for the specific volume. On classified documents enter the title classification in parentheses.

Block 5. Funding Numbers. To include contract and grant numbers; may include program element number(s), project number(s), task number(s), and work unit number(s). Use the following labels:

C	- Contract	**PR**	- Project
G	- Grant	**TA**	- Task
PE	- Program Element	**WU**	- Work Unit Accession No.

Block 6. Author(s). Name(s) of person(s) responsible for writing the report, performing the research, or credited with the content of the report. If editor or compiler, this should follow the name(s).

Block 7. Performing Organization Name(s) and Address(es). Self-explanatory.

Block 8. Performing Organization Report Number. Enter the unique alphanumeric report number(s) assigned by the organization performing the report.

Block 9. Sponsoring/Monitoring Agency Names(s) and Address(es). Self-explanatory.

Block 10. Sponsoring/Monitoring Agency. Report Number. (If known)

Block 11. Supplementary Notes. Enter information not included elsewhere such as: Prepared in cooperation with...; Trans. of ..., To be published in .... When a report is revised, include a statement whether the new report supersedes or supplements the older report.

Block 12a. Distribution/Availablity Statement. Denote public availability or limitation. Cite any availability to the public. Enter additional limitations or special markings in all capitals (e.g. NOFORN, REL, ITAR)

DOD - See DoDD 5230.24, "Distribution Statements on Technical Documents."
DOE - See authorities
NASA - See Handbook NHB 2200.2.
NTIS - Leave blank.

Block 12b. Distribution Code.

DOD - DOD - Leave blank
DOE - DOE - Enter DOE distribution categories from the Standard Distribution for Unclassified Scientific and Technical Reports
NASA - NASA - Leave blank
NTIS - NTIS - Leave blank.

Block 13. Abstract. Include a brief (Maximum 200 words) factual summary of the most significant information contained in the report.

Block 14. Subject Terms. Keywords or phrases identifying major subjects in the report.

Block 15. Number of Pages. Enter the total number of pages.

Block 16. Price Code. Enter appropriate price code (NTIS only).

Blocks 17. - 19. Security Classifications. Self-explanatory. Enter U.S. Security Classification in accordance with U.S. Security Regulations (i.e., UNCLASSIFIED). If form contains classified information, stamp classification on the top and bottom of the page.

Block 20. Limitation of Abstract. This block must be completed to assign a limitation to the abstract. Enter either UL (unlimited) or SAR (same as report). An entry in this block is necessary if the abstract is to be limited. If blank, the abstract is assumed to be unlimited.